

1 LncRNAs interacting with the translation machinery contribute to human neuronal differentiation

2

3 Katerina Douka<sup>1,2</sup>, Isabel Birds<sup>1,2</sup>, Dapeng Wang<sup>2</sup>, Sophie Clayton<sup>1,3</sup>, Abigail Byford<sup>1,3</sup>, Elton J. R.  
4 Vasconcelos<sup>2</sup>, Mary J. O'Connell<sup>5</sup>, Jim Deuchars<sup>2,3</sup>, Adrian Whitehouse<sup>1,2,4</sup> and Julie L. Aspden<sup>1,2</sup> #

5

6 <sup>1</sup> School of Molecular and Cellular Biology, Faculty of Biological Sciences, University of Leeds, LS2 9JT,  
7 UK.

8 <sup>2</sup> LeedsOmics, University of Leeds, UK

9 <sup>3</sup> School of Biomedical Sciences, Faculty of Biological Sciences, University of Leeds, LS2 9JT, UK.

10 <sup>4</sup> Astbury Centre for Structural Molecular Biology, University of Leeds, Leeds, LS2 9JT, UK.

11 <sup>5</sup> School of Life Sciences, Faculty of Medicine and Health Sciences, The University of Nottingham,  
12 Nottingham, NG7 2UH, UK.

13 # corresponding author: j.aspden@leeds.ac.uk

14

15 Abstract

16 LncRNAs are less conserved, yet more tissue and developmental-stage specific than mRNAs  
17 and are particularly enriched in the nervous system of *Drosophila melanogaster*, mouse and human.  
18 The function of cytoplasmic lncRNAs and their potential translation remains poorly understood. Here  
19 we performed Poly-Ribo-Seq to understand the interaction of lncRNAs with the translation machinery  
20 and the functional consequences during neuronal differentiation of SH-SH5Y cells. We discovered 237  
21 cytoplasmic lncRNAs upregulated during early neuronal differentiation, most of which are associated  
22 with polysome complexes. The majority are cytoplasmically enriched and are intergenic or anti-sense.  
23 In addition, we find 45 small ORFs in lncRNAs to be actively translated, 17 specifically upon  
24 differentiation. 11 of these smORFs exhibit high sequence conservation across *Hominidae* suggesting  
25 they are under strong selective constraint with putative function in this clade. We discover LINC01116  
26 is induced upon differentiation and contains an 87 codon smORF, which we detect as translated, with  
27 increased ribosome profiling signal upon differentiation. The LINC01116 peptide exhibits a  
28 cytoplasmic distribution and is detected in neurites. Knockdown of LINC01116 results in significant  
29 reduction of neurite length in differentiated cells indicating it contributes to neuronal differentiation.  
30 Our findings indicate lncRNAs are a source of non-canonical peptides and contribute to neuronal  
31 function.

32

33 Introduction

34 Long non-coding RNAs (lncRNAs) are >200nt and thought to lack the potential to encode  
35 proteins. LncRNAs are well known to play key roles in development and differentiation via several

36 mechanisms (Dimartino et al., 2018; Tsagakis et al., 2020), such as the base-pairing of lnc-31 with  
37 Rock1 mRNA, to promote its translation during myoblast differentiation (Dimartino et al., 2018). ~40%  
38 of human lncRNAs are specifically expressed in the brain (Derrien et al., 2012), where they display  
39 precise spatiotemporal expression profiles (Ponting et al., 2009). A subset of nuclear neuronal lncRNAs  
40 have been found to regulate neuronal differentiation in mouse and human (Carelli et al., 2019;  
41 Chodroff et al., 2010; Lin et al., 2014; Winzi, 2018). Until recently, the majority of work has focused on  
42 nuclear lncRNA functions, following the belief that most lncRNAs were retained in the nucleus (Derrien  
43 et al., 2012; Djebali et al., 2012). However, it has become increasingly clear that many lncRNAs are  
44 exported to the cytoplasm (Carlevaro-Fita et al., 2016) and have specific cytoplasmic functions in post-  
45 transcriptional gene regulation whilst some possess specific neuronal roles. For example, UCHL1-AS is  
46 detected in dopaminergic neurons and promotes translation of UCHL1 mRNA by increasing its  
47 association with heavy polysomes (Carrieri et al., 2012). Whereas BACE1-AS transcript, which is  
48 significantly upregulated in the brain of Alzheimer's disease patients, base-pairs with beta-secretase-  
49 1 (BACE1) mRNA, stabilising it by masking miR-485-5p binding sites (Faghihi et al., 2010). Alternatively,  
50 BC200 represses translation initiation in dendrites by disrupting the formation of pre-initiation 48S  
51 complexes (Wang et al., 2002).

52 Translation regulation is essential during neuronal differentiation (Mohammad et al., 2019),  
53 with the translation of non-canonical ORFs, e.g. upstream ORFs (uORFs), playing important roles (Blair  
54 et al., 2017; Fujii et al., 2017; Rodriguez et al., 2019). Ribosome profiling in a range of organisms and  
55 tissue types has revealed the translation of a variety of non-canonical ORFs including small ORFs  
56 (smORFs) <100 codons in length (Aspden et al., 2014; Blair et al., 2017; Duncan & Mata, 2014; Fujii et  
57 al., 2017; Guo et al., 2010; Ingolia et al., 2013; Rodriguez et al., 2019). Although these translation  
58 events remain controversial, it is clear that lncRNAs can interact with the translation machinery.  
59 Limited ribosome profiling signal found on smORFs might be the result of sporadic binding of a single  
60 ribosome and may not necessarily correspond to active translation. Poly-Ribo-Seq was previously  
61 developed to distinguish those lncRNAs that are bound by multiple ribosomes, and therefore actively  
62 translated, from such a background signal. Predicting which lncRNA-smORFs are translated has proven  
63 difficult, as attributes to predict protein-coding ability are ineffective on small non-canonical ORFs. A  
64 small but growing number of smORF peptides translated from lncRNAs have been found to exhibit  
65 cellular and organismal functions (Anderson et al., 2015; Chen et al., 2020; Magny et al., 2013; Pueyo  
66 & Couso, 2008; Spencer et al., 2020; Wang et al., 2020).

67 To study the dynamic interactions of lncRNAs with the translation machinery and identify  
68 actively translated cytoplasmic lncRNAs during early neuronal differentiation, we perform Poly-Ribo-  
69 Seq on SH-SY5Y cells (human neuronal cell line). During differentiation a global decrease in translation

70 is evident and ribosomal protein mRNAs are specifically excluded from the polysomes during  
71 differentiation as part of this down-regulation. We detect ~800-900 lncRNA genes in the cytoplasm of  
72 SH-SY5Y cells. Specifically, 237 lncRNAs are upregulated and 100 downregulated during  
73 differentiation, 58-70% of which interact with polysome complexes. These interactions are dynamic  
74 during differentiation. Ribo-Seq identified 45 actively translated smORFs in lncRNAs, several of which  
75 are regulated during differentiation. A subset of these translation events was validated by transfection  
76 tagging experiments and analysis of publicly available mass spectrometry data. High levels of sequence  
77 conservation across *Homimidae* indicates that the resulting lncRNA-smORF peptides are produced in  
78 other great apes and likely possess cellular functions. One of the lncRNA genes that we discover to be  
79 significantly upregulated during differentiation is LINC01116, which is cytoplasmically enriched and  
80 associated with polysomes. Our Ribo-Seq analysis reveals the translation of an 87aa peptide from  
81 LINC01116 with increased ribosome profiling coverage upon differentiation. The LINC01116 peptide  
82 exhibits a cytoplasmic distribution and is detected in neurites. We reveal that LINC01116 contributes  
83 to neuronal differentiation and is required for proper neurite lengthening.

84

85 **Results**

86 **Differentiation of SH-SY5Y cells with retinoic acid results in reduced translation levels**

87 To dissect the importance of cytoplasmic lncRNAs and their ribosome associations in early  
88 neuronal differentiation we profiled the differentiation of SH-SY5Y cells with retinoic acid (RA) for 3  
89 days. This treatment results in neuronal differentiation as indicated by neurite elongation (Sup 1A),  
90 which can be seen by immunostaining for neuronal βIII-tubulin (TuJ1) (Fig 1A). Quantification of  
91 neurite length reveals significant elongation upon RA treatment (Fig 1B). There is also increased  
92 expression of neuronal markers; more cells express c-Fos upon differentiation (Sup 1B, C). There is a  
93 concomitant reduction in cell proliferation, as seen by reduced number of Ki67+ cells (Sup 1D, Fig 1C)  
94 as well as a reduction in the levels of pluripotency marker SOX2 (Sup 1E). These differentiated cells  
95 exhibit characteristics of outer radial glia neural progenitors and are driven towards a noradrenergic  
96 phenotype as indicated by increased Dopamine Beta Hydroxylase like Monoxygenase Protein 1  
97 (MOXD1) expression (Sup 1F) (Pollan et al., 2015; Xin et al., 2004). Translational output assessment by  
98 polysome profiles (Fig 1D) reveals that differentiation results in down-regulation of global translation.  
99 Quantification of translation complexes across the sucrose gradients indicates that levels of polysomes  
100 are reduced with respect to 80S monosomes (Sup 1G) resulting in a reduced polysome to monosome  
101 ratio (Fig 1E). This down-regulation of translation is accompanied by a shift of ribosomal protein (RP)  
102 mRNAs from polysomes to monosomes; e.g. RpL26 mRNA (Fig 1F, Sup 1H), RpS28 (Sup 1I) and RpL37

103 (Sup 1J), as measured by RT-qPCR across gradient fractions. This reduced synthesis of RPs has  
104 previously been reported during neuronal differentiation (Blair et al., 2017; Chau et al., 2018).

105

106 **Poly-Ribo-Seq reveals differences in RNA expression and polysome association upon differentiation**

107 To profile RNA, ribosome association and translational changes upon differentiation we  
108 employed Poly-Ribo-Seq (Aspden et al., 2014) with some minor modifications to adapt to human  
109 neuronal cells (Fig 2A). This adaptation of ribosome profiling (Ribo-Seq) can detect which RNAs are  
110 cytoplasmic, polysome associated and translated (Fig 2A). We sequenced i) poly-A selected  
111 cytoplasmic RNA, ‘Total’ RNA-Seq, ii) Polysome-associated poly-A RNAs, ‘Polysome’ RNA-Seq, and iii)  
112 ribosomal footprints, Ribo-Seq, from control and RA differentiated cells, with three biological  
113 replicates (Materials and Methods for details).

114 PCA of the 3 Total and 3 Polysome RNA-Seq for both Control and RA treatment shows that RA  
115 treated samples cluster separately from Control samples and biological replicates generally cluster  
116 together (Sup 2A). To profile differences as a result of differentiation we compared Control and RA  
117 samples, performing differential expression analysis at the gene level for both Polysomal RNA-Seq  
118 samples (main figures) and Total Cytoplasmic RNA-Seq samples (supplemental figures). To dissect the  
119 ability of RNAs to associate with translation complexes we compared the “Polysomal” and “Total” RNA  
120 populations for both Control and RA conditions, again through differential expression analysis at the  
121 gene level. Differences in expression between Control and RA are greater than those seen between  
122 Total and Polysome populations. Interestingly the variation in gene expression between differentiated  
123 (RA) Total and Polysome is greater than the variation between Control Total and Control Polysome  
124 (Sup 2A).

125 Analysis of the two types of RNA-Seq revealed large changes in RNA expression in response to  
126 differentiation, as previously determined (Blair et al., 2017). In fact, 897 protein-coding genes are  
127 upregulated upon RA treatment and 732 downregulated, within the Polysomes (Fig 2B). A very similar  
128 pattern is seen from Total; 936 up-regulated and 691 down-regulated genes (Sup 2B), and 78% of the  
129 significantly affected protein-coding genes are in common between Total and Polysome populations  
130 (Sup 2C&D). GO term analysis of these differentiation-regulated protein-coding genes indicates that  
131 functions corresponding to neuronal differentiation are upregulated (Fig 2C). There is an enrichment  
132 of ribosome and translation functions in those genes downregulated upon neuronal differentiation  
133 (Fig 2D). A clearer enrichment of genes with neuronal functions is evident in GO analysis of Total RNA-  
134 Seq (Sup 2E), e.g. synaptic transmission and similar enrichment of translation functions are in the  
135 downregulated set (Sup 2F). Expression of genes required for neuronal differentiation is increased or

136 induced upon RA treatment, e.g. Secretogranin, which is involved in packaging of neuropeptides into  
137 secretory vesicles (Sossin & Scheller, 1991) (Fig 2E).

138 Comparison of Total and Polysome RNA-Seq indicates that some mRNAs are enriched in  
139 polysomes whilst others are depleted. Ribosomal protein mRNAs are specifically depleted from  
140 polysomes upon differentiation, as seen by their altered relative levels between Total and Polysomes  
141 in Control (Fig 2F) and RA (Fig 2G). This is consistent with a global downregulation in translation (Fig  
142 1D) and shift of RP mRNAs out of the polysomes (Fig 1F). By comparing these polysome enriched and  
143 depleted mRNAs between Control and RA the dynamic nature of polysome association during  
144 differentiation is revealed (Fig 2H). More mRNAs become depleted during differentiation, including  
145 more RP mRNAs. GO term analysis of those genes enriched or depleted in the polysomes (Sup 2G, H,  
146 I) supports this depletion of RP mRNAs upon differentiation (Sup 2I).

147

#### 148 **LncRNAs are induced and associated with polysomes during differentiation**

149 To understand the potential role and regulation of cytoplasmic lncRNAs we analysed their  
150 expression levels in Total and Polysome populations upon differentiation (Sup 3A). We detect large  
151 numbers of lncRNAs present in the cytoplasm. 801 lncRNA genes expressed and present (i.e. have  
152 RPKMs  $\geq 1$ ) in the cytoplasm under control conditions and 916 lncRNA genes in differentiated cells.  
153 Interestingly, 237 lncRNA genes were upregulated during differentiation whilst only 82 were  
154 downregulated, within Polysome fractions (Fig 3A). A very similar pattern was seen when considering  
155 Total RNA-seq with 178 lncRNA genes up-regulated and 100 down-regulated (Sup 3B). The majority of  
156 these differences were identified in both Total and Polysome populations (70% of the upregulated  
157 and 58% of the downregulated lncRNAs were in common between total and polysome) (Sup 3C&D).  
158 Interestingly when we look in more detail at these lncRNA regulated during differentiation the  
159 majority of differentiation-regulated lncRNAs are either intergenic or/and anti-sense lncRNAs (Fig 3  
160 B&C-Polysome, Sup 3 E&F-Total). Direct comparison of levels of lncRNAs within the whole cytoplasm  
161 and within polysome fractions indicates the vast majority lncRNAs (Control: 98% and RA: 99% are  
162 neither polysome enriched nor depleted (Sup 4 A&B). A small number (Control: 12 and RA: 10) of  
163 lncRNAs are specifically depleted from the polysomes including several lncRNAs derived from small  
164 nucleolar RNA host genes. Interestingly there is a smaller proportion of anti-sense lncRNAs within  
165 these polysome-depleted populations (Sup 4 C&D) compared to differences in expression during  
166 differentiation (Fig 3 B&C).

167 Significant induction of specific polysome-associated lncRNAs during differentiation, such as  
168 DLGAP1-AS2 is suggestive of a regulatory role during neuronal differentiation (Fig 3 A&D). We  
169 validated these differentiation-induced changes in a subset of 7 lncRNAs (Fig 2E). By RT-qPCR the

170 expression of all candidate lncRNAs were significantly upregulated upon differentiation, as was  
171 determined by RNA-Seq analysis. Fold-changes were highly correlative between RNA-Seq and RT-qPCR  
172 (Sup 4E). To enable us to focus on lncRNAs with potential neuronal functions we selected candidate  
173 lncRNAs that exhibited the highest fold increase in levels upon differentiation. The majority of these  
174 candidate lncRNAs (6/7) are specifically enriched in the cytoplasm, rather than the nucleus (Fig 3E,  
175 Sup 4F) in contrast to the known nuclear lncRNA Xist. Only 2/7 lncRNAs tested showed changes in  
176 cytoplasmic enrichment upon differentiation (Sup 4G), the majority do not (5/7). When these  
177 candidate lncRNAs were profiled across sucrose gradient fractions they were found to associate with  
178 polysome complexes within the cytoplasm. LINC02143, which is induced >22-fold during  
179 differentiation (Fig 3E), is highly enriched in the cytoplasm compared to the nucleus (Fig 3F) and is  
180 found in monosomes and small polysomes (Fig 3G). It is also just as upregulated in polysomes (Fig 3A)  
181 as in the total cytoplasm (Sup 3B) during differentiation. Unlike DLGAP1-AS2, DLGAP1-AS1 is enriched  
182 in the cytoplasm (Fig 3F) and associates with small polysomes, as well as ribosomal subunits (Sup 4H).

183 Another lncRNA whose levels significantly increase during differentiation is LINC01116 (Fig 3  
184 A&E), which is involved in the progression of glioblastoma (GBM) (Brodie et al., 2017). LINC01116 is  
185 enriched in the cytoplasm (Fig 3F), detected at high levels in the 80S (monosome) fraction and in small  
186 polysomal complexes (Fig 3H). Upon differentiation there is an increase in the amount of LINC01116  
187 present in disomes, compared to Control. This is consistent with the upregulation of LINC01116  
188 transcript in the polysomes detected by RNA-Seq, indicating a functional interaction of LINC01116  
189 with polysomes during differentiation. In fact, the majority of LINC01116 transcript was found to  
190 associate with polysomes in both undifferentiated (Control) cells (66%) and upon differentiation (RA-  
191 57%), suggesting it could either be translated or associating with translation complexes (Fig 3H).

192

### 193 Translation of lncRNA-smORFs during differentiation

194 To better understand the association of lncRNA with polysome complexes and their potential  
195 translation we analysed ribosome footprinting from our Poly-Ribo-Seq experiments (Fig 2A). Framing  
196 analysis reveals good framing, specifically at footprint lengths of 31 and 33 nt (Fig 4A) and discrete  
197 footprint lengths (Sup 5A). On average 95% of ribosome footprints mapped to CDSs, whilst in RNA-  
198 Seq this was only 53% (Sup 5B). Metagene analysis of 31 nt length reads indicates that framing is high  
199 within ORFs, and that the footprint signal outside of ORFs is mostly within 5'-UTRs rather than 3'-UTRs,  
200 where there is a sharp drop off in footprints at the stop codon (Sup 5C). Together these attributes  
201 indicate that our Ribo-Seq quality is high and represents genuine translation events. Since 31 and 33nt  
202 reads exhibited high triplet-periodicity they were selected for downstream analysis of translation  
203 events to identify ORFs that are translated (Fig 4B). Overall, we are able to detect 16,282 protein-

204 coding ORFs translated in Control and 12,745 in RA, 10,014 of which are translated in both conditions  
205 (Table 1). Interestingly we are also able to detect the translation of 71 uORFs and 5 dORFs (Table 1).

206

207 To monitor translational changes we performed differential translation analysis (Chothani et  
208 al., 2019). Differential ribosome occupancy on ORFs ( $\Delta$ RPF), differential mRNA expression ( $\Delta$ RNA) and  
209 differential translation efficiency ( $\Delta$ TE) were calculated (Chothani et al., 2019). The majority of  
210 changes in protein production are driven by transcriptional regulation during differentiation, with no  
211 change in TE (Fig 4C). We detected 3 protein-coding CDSs being exclusively regulated by translation,  
212 upon differentiation (Fig 4C). One of these is centromere protein S (CENPS), which is expressed at low  
213 levels in neuroblastoma tumours and is thought to reduce cell growth (Carén et al., 2005; Krona et al.,  
214 2004). We were also able to identify CDSs that are known to be regulated during differentiation such  
215 as cytochrome P450 26A1 and cytochrome P450 26B1 (CYP26A1, CYP26B1), involved in RA  
216 metabolism (Maden, 2007) (Fig 4D). These ORFs are transcriptionally and translationally upregulated,  
217 and their TE is significantly increased upon differentiation.

218 Importantly, using our pipeline (Fig 4B) we also detect the translation of 45 ORFs within  
219 lncRNAs, 28 in control and 23 during differentiation, 6 of these were translated in both conditions (Fig  
220 4E). Interestingly, TEs for these lncRNA-smORFs are similar to those of protein-coding ORFs (Fig 4F),  
221 providing further evidence that these are genuine translation events. The dORFs that we detect are  
222 translated at much lower efficiencies (Fig 4F). This makes sense considering that ribosomes will likely  
223 have to reinitiate after the main ORF, which will occur at a low efficiency. One of the lncRNA-smORFs  
224 we identify to be translated in differentiated cells, has previously been characterised, the 84 aa  
225 CRNDEP (Szafron et al., 2015). Analysis of these 45 translated smORFs from lncRNAs shows that they  
226 are <300 aa in length with a median size of 56 aa in Control and 64 aa in RA (Fig 4G, Sup 5D).

227 Previous analysis has indicated that smORF peptides exhibit specific amino acid usage, which  
228 suggests they are both genuine proteins and show enrichment for transmembrane alpha-helices (Song  
229 et al., 2010). Therefore, we profiled the amino acid composition of our lncRNAs-smORFs, uORFs and  
230 dORFs compared to protein-coding ORFs and expected frequency (Fig 4H). lncRNA-smORFs exhibit  
231 similar frequencies to known protein-coding ORFs. Specifically, smORFs possess lower than expected  
232 arginine levels, but not as low as known protein-coding ORFs. Amino acid usage does not suggest that  
233 any smORF groups have propensity to form transmembrane alpha-helices (Aspden et al., 2014).

234 From within the set of lncRNAs we identified as induced during differentiation, several  
235 contained translated smORFs. One of these is LINC01116, whose translated ORF exhibits high framing  
236 (Fig 4I). In fact, ~80% of reads that map to this ORF are in frame 2, whereas outside this ORF, the few  
237 reads mapping to the remaining lncRNA sequence are far more equally distributed between the three

238 possible frames (Fig 4I). This smORF is 71-codons, and its start codon is 608nt into the lncRNA.  
239 Ribosome profiling signal is substantially higher upon differentiation, mainly as a result of increased  
240 lncRNA transcript abundance (Sup 5E).

241

#### 242 Peptide synthesis from smORFs in lncRNAs during differentiation

243 Our pipeline is highly stringent, i.e., there are many additional ORFs that display good framing  
244 but do not pass our thresholds for numbers of footprinting reads or exhibit background signal in rest  
245 of the lncRNA. Therefore, we are confident these translation events are taking place. To validate  
246 peptide synthesis, we have taken two complementary strategies; mass spectrometry analysis and  
247 transfection of ORF tagging constructs. Mass spectrometry generally only detects 90% of translated  
248 proteins from protein-coding genes (Zubarev, 2013). Analysis of previously published mass  
249 spectrometry datasets from SH-SY5Y (undifferentiated and RA-treated) cells (Brenig et al., 2020;  
250 Murillo et al., 2018) supports the production of peptides from 6 of our translated uORFs (2 Control, 4  
251 RA) and 8 lncRNA-smORFs (4 Control and 4 RA) (Fig 5A). This represents ~8% (uORFs) and 18% (lncRNA-  
252 smORFs) of what is detected in Poly-Ribo-Seq. This is to be expected given the small size of these  
253 peptides and therefore reduced chance of producing peptides >8aa from digestion for mass  
254 spectrometry detection (Saghatelyan & Couso, 2015).

255 To validate translation of our lncRNA-smORFs that were not identified in previous mass  
256 spectrometry but were detected as translated by our Poly-Ribo-Seq analyses, we have also used a  
257 transfection tagging approach. We cloned the lncRNA sequence to the 5' of the putative ORF, termed  
258 the 5'-UTR and the smORF itself, without its stop codon, with a C terminal 3x FLAG tag (Fig 5B). The  
259 start codon of this FLAG tag is deleted, so any FLAG signal is the result of translation from the lncRNA-  
260 smORF. Two candidate lncRNA-smORFs were selected that did not have mass spectrometry support;  
261 LINC000478 and LINC01116. A 37 codon smORF was detected as translated from LINC00478 in both  
262 conditions (Fig 5C). Transfection of LINC00478-smORF-FLAG into undifferentiated SH-SY5Y cells  
263 produced FLAG signal in both nuclear and cytoplasmic compartments (Fig 5D & Sup 6A). FLAG signal  
264 was also seen when LINC00478-smORF-FLAG transfected SH-SY5Y cells were treated with RA (Sup 6A).  
265 Interestingly this RA FLAG signal was only ever detected in the nucleus. Similar results were seen in  
266 HEK293 cells (Sup 6B), but because of the higher transfectional efficiency in HEK293 compared with  
267 SH-SY5Y cells, we detect FLAG signal in more cells.

268 Poly-Ribo-Seq detected increased levels of LINC01116 during differentiation (4-fold in Control  
269 vs RA polysome) and translation of a 71-codon smORF during differentiation (Fig 4I). Tagging of  
270 LINC01116-smORF (Fig 5E) generated FLAG signal in the cytoplasm of SH-SY5Y cells, which is localized  
271 to neurites (Fig 5F), suggesting it could play a role in differentiation. FLAG signal was also present in

272 LINC01116 transfections in HEK293 cells (Sup 6C), but because of the higher transfectional efficiency  
273 in HEK293 compared with SH-SY5Y cells, we detect FLAG signal in more cells.

274 LINC01116-smORF has two potential ATG start codons (Fig 5E and Sup 6D). When these start  
275 codons were assessed for similarity to the Kozak sequence consensus, using NetStart1.0 (Pedersen &  
276 Nielsen, 1997), both exhibited scores >0.5, indicating both are in good context and therefore either  
277 could be used to initiate translation (AUG<sub>1</sub>= 0.545, AUG<sub>2</sub>= 0.645). Given the scanning model of  
278 translation initiation it seems likely that the first AUG would be used. To determine if the first start  
279 codon is actually used it was mutated (Fig 5E). No FLAG signal was present in transfections where the  
280 5' start codon was mutated ( $\Delta 1$ ) (Fig 5G). This suggests that the first start codon is necessary for the  
281 translation of the LINC01116-smORF and the resulting peptide is 87aa long. Although FLAG signal is  
282 present in a low number of cells, no transfection controls and  $\Delta 1$  indicate that FLAG signal is  
283 dependent on translation of the LINC01116-smORF (Sup 6E).

284

## 285 **Translated lncRNA-smORFs exhibit sequence conservation**

286 Another indicator of coding potential and also of peptide functionality is the sequence  
287 conservation of our translated lncRNA-smORFs. To ensure detection of sequence conservation for  
288 these short smORFs irrespective of annotation in other genomes, we used three complementary  
289 BLAST strategies using transcript nt sequence, smORF nt sequence and protein aa sequence.

290 Initial searches using the entire lncRNA transcript sequence (nt) and BLASTn (Altschul et al.,  
291 1990), returned results for ~78% of translated lncRNAs, many of which had short alignment lengths of  
292 30-100 nt. Although some of these results may represent conservation of the smORFs, many are due  
293 to small areas of sequence overlap along the rest of the lncRNA. This is a well-documented issue when  
294 investigating lncRNAs; they rarely exhibit the same levels of conservation as mRNAs (Johnsson et al.,  
295 2014). A more common finding is that there are “modules” of higher sequence conservation across  
296 lncRNA transcripts, as described for Xist lncRNA (Brockdorff, 2018). To accommodate this, a second  
297 round of searches were performed, on the initial search results, using the nt sequence of the smORF  
298 (BLASTn) (Altschul et al., 1990). This filtering step resulted in fewer, higher quality results, with 14 of  
299 18 remaining lncRNA-smORFs passing manual cross validation. For the majority of the these lncRNA-  
300 smORFs, conservation is high across the body of the smORF, and drops off across the rest of the  
301 transcript. The ENST00000442428.1 (AL162386.2)-smORF exhibits high sequence conservation when  
302 compared to gorilla and orangutan (*Pongo abelii*), with 100% and 99% ORF nt sequence identity  
303 respectively (Figure 5H). When entire transcripts are aligned, this percentage sequence identity drops  
304 to 74% with gorilla (ENSGGOT00000060708.1), and 65% with orangutan (ENSPPYT00000022401.2),  
305 indicating the ORF is the most conserved part of these transcripts.

306 To further corroborate these results, a tBLASTn (Altschul et al., 1990) search of the lncRNA-  
307 smORF aa sequences was performed. By translating transcript databases into aa in all 6 frames,  
308 tBLASTn removes the noise of synonymous substitutions, which can have a significant effect,  
309 particularly in smORFs (Ladoukakis et al., 2011). For the majority of smORFs, the same results were  
310 returned, and evidence of conservation was found for a further three lncRNA-smORFs  
311 (ENST00000454935.1\_477\_633, ENST00000557660.5\_42\_186, ENST00000453910.5\_151\_262) that  
312 appear to have undergone some frameshift mutations.

313 At the aa sequence level, ~18% of the translated lncRNA-smORFs returned homologous  
314 proteins from BLASTp searches (Altschul et al., 1990). All the returned proteins were unreviewed,  
315 uncharacterised proteins, with no evidence at protein, transcript or homology levels in the Uniprot  
316 database (Bateman et al., 2019). This potentially suggests that automated annotation pipelines  
317 recognised the coding potential of these smORFs, unlike in the more curated human genome  
318 annotation. Overall, the combination of these 3 layers of sequence conservation analysis reveal that  
319 11 of our translated lncRNA-smORFs exhibit sequence conservation across *Hominidae*, 3 addition  
320 smORFs are also found in gibbons (Fig 5I), with evidence for 2 translated smORFs detectable at the  
321 greater evolutionary distance of human to mouse, but not found in all apes (Sup 6E).

322

### 323 **LINC01116 contributes to neuronal differentiation**

324 To dissect the potential role of LINC01116 and its translation during differentiation we  
325 knocked down LINC01116 using a siRNA pool in both undifferentiated and differentiated SH-SY5Y cells  
326 (Fig 6A). LINC01116 knockdown initially had a limited effect on cell viability, which recovered to no  
327 effect after 2 days (Sup 7A). Interestingly, LINC01116 knockdown resulted in a significant reduction of  
328 neurite length in RA treated SH-SY5Y cells (Fig 6B, zoom in Fig 6C), compared to scrambled siRNA  
329 treated SH-SY5Y (Fig 6D). There was no effect of the knockdown in undifferentiated cells (Fig 6D). This  
330 suggests that LINC01116 is involved in the regulation of neuritic processes formation. To examine  
331 potential effects of LINC01116 knockdown further on differentiation we assessed the expression levels  
332 of the noradrenergic marker MOXD1, which is important in neural crest development. LINC01116  
333 siRNA knockdown, upon differentiation resulted in a reduction of MOXD1 expression levels, further  
334 indicating a role of LINC01116 in neuronal differentiation (Fig 6E). However, LINC01116 knockdown had  
335 no effect on proliferation, as measured by % of Ki67+ cells (Sup 7B & Fig 6F) or cell cycle, as measured  
336 by E2F1 mRNA RT-qPCR (Fig 6G). LINC01116 likely functions early in the differentiation pathway since  
337 its levels are significantly upregulated within the first 24 hours of RA induced differentiation (Sup 7C).  
338 Expression of LINC01116 then declines rapidly by day 8 (Fig 7D). Together these results suggest that  
339 LINC01116 functions during early differentiation, contributing to neurite process formation.

340

341

342 Discussion

343 Cytoplasmic lncRNAs have recently emerged as important regulators of several cellular  
344 processes, including the regulation of translation, in a variety of tissues (Carrieri et al., 2012; Dimartino  
345 et al., 2018). Moreover, the active translation of smORFs from within lncRNAs has been characterized  
346 in a range of organisms (Anderson et al., 2015; Aspden et al., 2014; Chen et al., 2020; Magny et al.,  
347 2013; Pueyo & Couso, 2008; Wang et al., 2020). Translational regulation is a key process during  
348 neuronal differentiation (Blair et al., 2017; Chau et al., 2018), therefore we reasoned that lncRNAs  
349 may functionally interact with polysomes during differentiation.

350 Having established that early neuronal differentiation of human neuroblastoma cells (SH-  
351 SY5Y) results in reduced global translation, we sought to further investigate the relationship of  
352 lncRNAs with the translation machinery during differentiation. We detected the presence of ~800-900  
353 lncRNA genes expressed and their transcripts present in the cytoplasm. 85-90% of these cytoplasmic  
354 lncRNAs are associated with polysome complexes, suggesting that they are either being translated, or  
355 regulating the translation of the mRNAs with which they interact. Moreover, the association of  
356 lncRNAs with polysomes is dynamic during differentiation, as shown by the differential polysome  
357 enrichment of lncRNAs in Control and RA treated cells. The lncRNAs that dynamically interact with  
358 polysomes upon neuronal differentiation mainly belong to the 'intergenic' and 'anti-sense' categories  
359 of lncRNAs. These results reveal that many lncRNAs are present in the cytoplasm, enriched there, and  
360 are associated with translation complexes.

361 An example of a polysome-associated lncRNA that we characterized in more detail is  
362 LINC02143. It is an intergenic lncRNA with no known function, which we find induced upon  
363 differentiation. It is detected in 80S and small polysome fractions, indicating it interacts with the  
364 translation machinery. A number of anti-sense polysome-associated lncRNAs appear to be  
365 upregulated upon differentiation. Amongst them is DLGAP1-AS1, which is anti-sense to Disks large-  
366 associated protein 1 (DLGAP1), itself involved in chemical synaptic transmission. DLGAP1-AS1 interacts  
367 with actively translating polysomes both in Control and upon differentiation. The lncRNAs depleted  
368 from the polysomes have fewer anti-sense lncRNAs relative to other populations, suggesting that anti-  
369 sense lncRNAs are preferentially localised to polysomes. These polysome associated anti-sense  
370 lncRNAs could potentially regulate the translation of their 'sense' mRNA, through base-pairing, as is  
371 the case with BACE1-AS (Faghihi et al., 2010) and UCHL1-AS (Carrieri et al., 2012). This contrasts with  
372 the general view that anti-sense lncRNAs regulate gene expression in the nucleus at the point of  
373 transcription or splicing (Beckedorff et al., 2013).

374 Differential translation analysis revealed that upon RA induced neuronal differentiation of SH-  
375 SY5Y for 3 days, a small number of ORFs are exclusively translationally regulated. For the majority of  
376 ORFs, translation regulation is driven by transcription regulation. This result indicates that at this early  
377 timepoint, transcriptional control, rather than translational control is the driving force of SH-SY5Y  
378 differentiation. This is not surprising, because according to a previous study of human embryonic stem  
379 cells (hESCs) differentiation into neural progenitor cells (NPCs) only 12% of the detected transcripts  
380 were exclusively translationally regulated (Blair et al., 2017).

381 Ribosome profiling of the actively translating polysomes allowed us to distinguish between  
382 the lncRNAs that associate with the polysome complexes and those that are being actively translated.  
383 We were able to identify 45 translated lncRNA-smORFs in undifferentiated and differentiated cells.  
384 Only ~5% of polysome-associated lncRNAs pass our stringent thresholds for translation. The translated  
385 lncRNA-smORFs exhibit high levels of triplet periodicity and their translational efficiencies are similar  
386 to those of protein-coding genes. We can therefore be confident that these are real translation events  
387 leading to the production of substantial peptide levels rather than background, spurious events  
388 (Bazzini et al., 2014; Guttman et al., 2013; Patraquim et al., 2020; Ruiz-Orera & Alba, 2019). The size  
389 distribution of our novel translated ORFs, indicates that the majority are indeed smORFs (<100aa). The  
390 general pattern we identified is that dORFs>lncRNA-smORF>uORFs in size. This is consistent with  
391 previous studies where a wide range of peptides lengths were discovered (Aspden et al., 2014; Chong  
392 et al., 2020). Amino acid composition of these translated smORFs supports the fact they are translated  
393 into peptides. However, it does not suggest they are enriched for transmembrane alpha-helices. This  
394 is in contrast to the smORFs characterized in *D. melanogaster* (Aspden, 2014).

395 Overall, we have independent evidence for peptide synthesis for 12/45 lncRNA-smORFs. 8 of  
396 these from published mass spectrometry data from Control and RA-differentiated cells SH-SY5Y cells  
397 (Brenig et al., 2020). In general, we find smORFs translated in the same treatment as these mass  
398 spectrometry datasets detect peptides (7/8). An 18% mass spectrometry detection level may seem  
399 low but given the limitations of detecting small peptides by mass spectrometry this represents a  
400 substantial level of validation. Two translation events were validated by FLAG tagging transfection  
401 assay: LINC01116 and LINC00478 lncRNA-smORFs. The production of 2/45 lncRNA-smORF peptides is  
402 corroborated by previous studies in non-neuronal cells. HAND2-AS1 (translated in Control and RA) is  
403 translated in human and rodent heart and encodes for an integral membrane component of the  
404 endoplasmic reticulum (van Heesch et al., 2019). CRNDE, which is only translated upon differentiation,  
405 encodes for a previously characterised nuclear peptide (CRNDEP) (Szafron et al., 2015). The translation  
406 of these smORFs in multiple cell types provides substantial support for the production of peptides and  
407 their potential function.

408 We also discovered that 24% of the lncRNA-smORFs we find translated show sequence  
409 conservation across the *Hominidae*. This suggests that the other great apes have the potential to  
410 translate very similar peptides. This provides additional evidence to indicate that these translation  
411 events are not translational noise. Of course, it will be interesting to uncover the function of these  
412 small peptides in the future.

413 Here we have discovered that LINC01116 produces an 87aa peptide that exhibits cytoplasmic  
414 localisation, and specifically is detected in near the cell membrane and in neuritic processes. The  
415 upregulation of LINC01116 expression upon differentiation as well as the existing evidence of its  
416 expression in the developing and adult brain and spinal cord (Consortium, 2013; Lindsay et al., 2016),  
417 coupled with the localisation of its peptide, led us to further investigate its potential role in  
418 differentiation. Knockdown of LINC01116 upon differentiation appears to impede neurite outgrowth  
419 and results in the reduction of the mRNA levels of the noradrenergic marker MOXD1. Our data suggest  
420 that LINC01116 is involved in the regulation of neuronal differentiation, consistent with the fact that  
421 it is moderately expressed in the developing human forebrain and highly expressed in the developing  
422 human midbrain and spinal cord (Lindsay et al., 2016). LINC01116 was previously found to be involved  
423 two other cancer models; in the progression of glioblastoma (Brodie et al., 2017) and it is upregulated  
424 in gefitinib resistant non-small cell lung cancer cells (Wang He et al., 2020). siRNA knockdown of  
425 LINC01116 in both these cell types results in decreased expression of stem-cell markers (Nanog, SOX2  
426 and Oct4) and reduced cell proliferation. This suggests LINC01116 promotes cell proliferation in these  
427 systems, indicating that the downstream effects of LINC01116 may vary according to cell type.  
428 Interestingly however, knockdown of LINC01116 also inhibited migration of glioma stem cells (GSCs)  
429 (Brodie et al., 2017), while overexpression of LINC01116 promoted invasion and migration of gastric  
430 cancer cells (Su et al., 2019). This suggests a potential role of LINC01116 in the formation of cell  
431 membrane protrusions, which is consistent with the role we have discovered for LINC01116 in neurite  
432 development.

433 Our findings indicate that many lncRNAs are localised in the cytoplasm and play important  
434 roles here. Given the large number of lncRNAs associated with polysomes we anticipate that many  
435 more lncRNAs will be found to regulate translation. We have identified 121 novel translation events,  
436 many of which are regulated during differentiation. Only ~5% of polysome-associated lncRNAs are  
437 translated. The lncRNA-smORFs we discover here represent a general population whose products  
438 have not yet been characterized. As we have found for LINC01116, lncRNAs and the small peptides  
439 encoded therein have the potential to contribute to important cellular functions and contribute to  
440 development and disease.

441

442 **Materials and Methods**

443 **Cell culture**

444 Human neuroblastoma SH-SY5Y cells, were cultured in Dulbecco's Modified Eagle Medium  
445 (DMEM 4.5g/L Glucose with L-Glutamine) supplemented with 1% (v/v) Penicillin/Streptomycin and  
446 10% Fetal Bovine Serum (FBS) at 37°C, 5% CO<sub>2</sub>. Neural induction commenced at passage 4 and was  
447 performed as described previously (Forster et al., 2016; Korecka et al., 2013) with minor alterations.  
448 All trans Retinoic Acid (RA, Sigma) was added to cells 24h after plating, at final concentration of 30μM.

449

450 **Immunocytochemistry**

451 Cells were seeded on Poly-D-Lysine/mouse laminin coated 12mm round coverslips (Corning  
452 BioCoat™ Cellware) and fixed with 4% paraformaldehyde (PFA) (Affymetrix) for 20 min at room  
453 temperature (RT). A permeabilization step (0.1% Triton-X for 10 min at RT) was performed prior to  
454 blocking, followed blocking at RT in blocking buffer (3% BSA, 1XPBS or 5% NGS, 1XPBS and 0.1% Triton-  
455 X) for 30 min. Primary antibodies (Antibody Table) were applied in (3% BSA 1X PBS or 0.5% NGS, 1X  
456 PBS, 0.1% Triton-X and incubated at RT for 2h or at 4° C overnight. Cells were washed and labelled  
457 with Alexa 488, Alexa 555, or Alexa 633 at 1:500 dilution for 2h at RT in 0.5% NGS, 1X PBS, 0.1% Triton-  
458 X. Cells were mounted in VECTASHIELD mounting medium, analysed using LSM 700 confocal  
459 microscope (Zeiss) ImageJ.

460

461 **cDNA synthesis and quantitative Real Time PCR (RT-qPCR)**

462 Equal amounts of RNA (whole cell, nuclear and cytoplasmic lysates) or equal volumes  
463 (polysome fractions) were subject to cDNA synthesis, using qScript (Quanta Bio) according to  
464 manufacturer's instructions. qPCR was performed using the CFX Connect™ thermal cycler and  
465 quantification using SYBR Green fluorescent dye (PowerUp™ SYBR Green Master Mix, Thermo Fisher  
466 SCIENTIFIC). Primers were designed to anneal to exon-exon junctions, where possible, or to common  
467 exons between alternative transcripts (Primer Table). Target mRNA and lncRNA levels were assessed  
468 by absolute quantification, by the means of standard curve or relative quantification, using the ΔΔCq  
469 method.

470

471 **Polysome Profiling**

472 RA was added to SH-SY5Y cells 3 days prior to harvesting. Cells were treated with  
473 cycloheximide (Sigma) at 100μg/ml for 3 min at 37°C, washed (1X PBS, 100μg/ml cycloheximide) and  
474 trypsinised for 5 min at 37°C. Subsequently, cells were pelleted, washed (1X PBS, 100μg/ml  
475 cycloheximide), and resuspended in ice cold lysis buffer; 50mM Tris-HCl pH8, 150mM NaCl, 10mM

476 MgCl<sub>2</sub>, 1mM DTT, 1% IGEPAL, 100µg/ml cycloheximide, Turbo DNase 24U/µL (Invitrogen), RNasin Plus  
477 RNase Inhibitor 90U (Promega), cOmplete Protease Inhibitor (Roche), for 45 min. Cells were then  
478 subjected to centrifugation at 17,000 xg for 5 min, to pellet nuclei. Cytoplasmic lysates were loaded  
479 onto 18%-60% sucrose gradients (~70 x10<sup>6</sup> cells per gradient) at 4°C and subjected to  
480 ultracentrifugation (121,355 x g<sub>avg</sub> 3.5h, 4°C) in SW-40 rotor. Gradients were fractionated using  
481 GRADIENT STATION (Biocomp) and absorbance at 254 nm was monitored using a Biorad detector.  
482

#### 483 **Poly-Ribo-Seq**

484 ~20% of cytoplasmic lysate was kept for PolyA selection (Total RNA control) and ~80% was  
485 loaded onto 18%- 60% sucrose gradients (~70x10<sup>6</sup> cells per gradient) at 4°C and subjected to  
486 ultracentrifugation (121,355 x g<sub>avg</sub> 3.5h, 4°C) in SW-40 rotor. Polysome fractions were pooled from  
487 control and from differentiated cells. ~25% polysomes were kept for polyA selection (Polysome-  
488 associated RNA). The remaining 75% was diluted in 100mM Tris-HCl pH8, 30mM NaCl, 10mM MgCl<sub>2</sub>.  
489 RNasel (EN601, 10U/µl 0.7-1U/million cells) was subsequently added incubated overnight at 4°C.  
490 RNasel was deactivated using SUPERase inhibitor (200U/gradient) for 5min at 4°C. Samples were  
491 concentrated using 30 kDa molecular weight cut-off columns (Merck) and loaded on sucrose cushion  
492 (1M sucrose, 50mM Tris-HCl pH8, 150mM NaCl, 10mM MgCl<sub>2</sub>, 40U RNase Inhibitor) and subjected to  
493 ultracentrifugation at 204,428 x g<sub>avg</sub> at 4°C for 4h (TLA110). Pellets were resuspended in TRIzol  
494 (Ambion, Life Technologies) and processed for RNA purification.

495 RNA purification from cytoplasmic lysates and RNasel footprinted samples was performed by  
496 Trizol RNA extraction, following manufacturer's instructions. RNA purification from polysome  
497 fractions was performed by isopropanol precipitation, followed by TURBO DNase treatment  
498 (Thermofisher) (according to manufacturer's instructions), acidic phenol/chloroform RNA purification  
499 and ethanol precipitation at -80°C overnight. RNA concentration was determined by Nano-drop 2000  
500 software. Two rounds of polyA selection from total cytoplasmic lysate and polysome fractions were  
501 performed using oligo (dT) Dynabeads (Invitrogen) according to manufacturer's instructions. PolyA  
502 RNA was fragmented by alkaline hydrolysis. 28–34 nt ribosome footprints and 50–80 nt mRNA  
503 fragments were gel purified in 10% (w/v) polyacrylamide-TBE-Urea gel at 300V for 3.5h in 1X TBE.  
504 Ribosome footprints were subjected to rRNA depletion (Illumina RiboZero rRNA removal kit).

505 5' stranded libraries were constructed using NEB Next Multiplex Small RNA Library Prep.  
506 Resulting cDNA was PCR amplified and gel purified prior to sequencing. Libraries were subjected to  
507 75bp single end RNA Seq using NextSeq500 Illumina sequencer, High Output Kit v2.5 (75 Cycles) (Next  
508 Generation Sequencing Facility, Faculty of Medicine, University of Leeds).  
509

#### 510 **RNA-Seq data analysis**

511 RNA-Seq reads were trimmed with Cutadapt (Martin, 2011) and filtered with  
512 fastq\_quality\_filter (Hannon, 2010) to filter out the reads of low quality (90% of the read to have a  
513 phred score above 20). Filtered reads were mapped (Liao et al., 2013) to human genome reference  
514 (the lncRNA GENCODE (Frankish et al., 2019) annotation added to mRNA annotation from UCSC  
515 (Haeussler et al., 2019) human genome assembly (hg19) from iGenomes) with Rsubread (Liao et al.,  
516 2013) and uniquely mapped reads were reported. Bam file sorting and indexing was performed with  
517 SAMtools (Li et al., 2009). Subsequently summarised read counts for all genes were calculated using  
518 featureCounts (Liao et al., 2014). For normalization, RPKM values were calculated. Differential  
519 expression analysis was conducted between with DESeq2 (Love et al., 2014) based on the two cut-offs  
520  $p^{\text{adj}} < 0.05$  and the absolute value of  $\log^2\text{FoldChange} > 1$ . Gene ontology analysis was performed with  
521 GOrilla (*Gene Ontology enRICHment anaLysis and visuaLizAtion tool*) (Eden et al., 2009).

522

### 523 **Cytoplasmic/Nuclear fractionation of SH-SY5Y cells.**

524 Cells were harvested (as above) and washed with 1X PBS. Cells were lysed in whole cell lysis  
525 buffer (see table) (500 $\mu$ L buffer per  $10^6$  cells) on ice for 30min. Whole cell lysate aliquots were  
526 removed and remainder subjected to centrifugation at 1,600 x g for 8 min to pellet nuclei. Nuclear and  
527 cytoplasmic fractions were subjected to two further clearing steps by centrifugation (3,000 x g and  
528 10,000 x g respectively). Nuclei were lysed in RIPA buffer (table). ~10% of both nuclear and cytoplasmic  
529 lysates were used for Western Blot and ~90% subjected to RNA extraction (ZYMO R1055).

530

### 531 **Western Blot**

532 Samples were diluted in 4X Laemmli sample buffer (Biorad) (277.8 mM Tris-HCl, pH 6.8, 4.4%  
533 LDS, 44.4% (v/v) glycerol, 0.02% bromophenol blue), 5%  $\beta$ -mercaptoethanol (Sigma) was added prior  
534 to heating at 95°C for 5 min and loaded on 10% SDS gels. Gel electrophoresis was performed using the  
535 BioRad Mini-PROTEAN 3 gel electrophoresis system (Bio-Rad Laboratories, Hercules, CA, USA).  
536 Proteins were transferred to nitrocellulose membranes (Amersham™ Protran™) and blocked with 5%  
537 fat-free milk powder in 1XPBS, 0.05% Tween-20 (Sigma) for 1h at RT. Blots were incubated with  
538 primary antibodies overnight (Antibody Table). Blots were then washed in PBS-T and incubated with  
539 secondary antibody (anti-mouse HRP) at RT for 2h. Membranes were washed 3 times with PBS-T, prior  
540 to application of ECL (Biological Industries). Chemiluminescent signal was detected with Chemi-Doc  
541 (BIO-RAD). All membranes were probed for  $\beta$ -tubulin as loading control.

542

### 543 **Ribo-Seq analysis**

544 Quality reports of Polysome-associated RNA-Seq and Ribo-Seq data were made using Fastqc  
545 (v.0.11.8) (Andrews, 2010). Adaptor sequences were trimmed using Cutadapt (v.1.81) (Martin, 2011)  
546 with minimum read length of 25bp, and untrimmed outputs retained for Ribo-Seq reads. Low-quality  
547 reads (score <20 for 10% or more of read) were then discarded using FASTQ Quality Filter, FASTX-  
548 Toolkit (v.0.0.14) (Gordon, 2010). Human rRNA sequences were retrieved from RiboGalaxy (Michel et  
549 al., 2016) and high confidence hg38 tRNA sequences from GtRNAdb Release 17 (Chan & Lowe, 2016).  
550 One base was removed from 3' end of reads to improve alignment quality, reads originating from  
551 rRNA and tRNA were aligned and removed using Bowtie2 (v.2.3.4.3) (Langmead & Salzberg, 2012).

552 The splice aware aligner STAR (v2.6.1b) (Dobin et al., 2012) was used to map remaining reads  
553 to human reference genome Release 30 (GRCh38.p12), from Gencode (Frankish et al., 2019). The STAR  
554 (v2.6.1b) (Dobin et al., 2012) genome index was built with a sjdbOverhang of 73. Samtools (v.1.9) (Li  
555 et al., 2009) was used to create sorted, indexed bam files of the resulting alignments.

556 Metaplots of aligned Ribo-seq data were generated using create\_metaplots.bash script from  
557 Ribotaper (v1.3) (Calviello et al., 2016) pipeline. These show the distance between the 5' ends of Ribo-  
558 seq and annotated start and stop codons from CCDS ORFs, allowing the locations of P-sites to be  
559 inferred. Read lengths exhibiting the best triplet periodicity were selected for each replicate, along  
560 with appropriate offsets (Sup 5).

561 Actively translated smORFs were then identified using Ribotaper (v1.3) (Calviello et al., 2016).  
562 Initially, this requires an exon to contain more than 5 P-sites in order to pass to quality control steps.  
563 Identified ORFs were then required to have a 3-nt periodic pattern of Ribo-seq reads, with 50% or  
564 more of the P-sites in-frame. In the case of multiple start codons, the most upstream in-frame start  
565 codon with a minimum of five P-sites in between it and the next ATG was selected.

566 ORFs for which >30% of the Ribo-seq coverage was only supported by multimapping reads were  
567 also subsequently filtered. For a smORF to be considered actively translated in a condition, we  
568 required that it be identified in at least two of the three biological replicates for the condition.

569  
570 **Translation efficiency calculation**

571 Translational efficiency (TE) was estimated for all translated ORFs in each condition, where TE  
572 was equal to the mean number of P sites per ORF, normalised by the median P sites per ORF per  
573 replicate, divided by the mean number of RNA sites per ORF, normalised by the median RNA sites per  
574 ORF per replicate.

575

576 **Differential translation efficiency analysis**

577 Differential translation efficiency analysis was performed using the ΔTE (Chothani et al., 2019)  
578 alternate protocol. However, our analysis was based on read counts from all identified translated ORFs  
579 from the Ribo-seq and polysome-associated RNA-seq, not the whole CDS as described in the protocol.  
580

#### 581 **Amino acid composition**

582 For each of our ORF sets (protein coding, lncRNA-smORF, uORF and dORFs), the average amino  
583 acid compositions were calculated. Random control expected frequencies were taken from King and  
584 Jukes (King & Jukes, 1969).

585

#### 586 **Mass spectrometry analysis**

587 Two published SH-SY5Y cell mass proteomics datasets were analysed: PXD010776 (Murillo et  
588 al., 2018) and PXD014381 (Brenig et al., 2020). Binary raw files (\*.raw) were downloaded from PRIDE  
589 then converted to human-readable MGF format using ThemoRawFileParser (Hulstaert et al., 2020).  
590 The amino acid sequences of our translated uORFs, dORFs and lncRNA-smORFs were added to the  
591 whole *Homo sapiens* proteome dataset (20,379 entries) downloaded from UniProtKB (Bateman et al.,  
592 2019) on Nov/2019. The new FASTA file was then used as a customized database on Comet  
593 (v2019.01.2) (Eng et al., 2013) search engine runs that scanned all MS/MS files (\*.mgf) against it.

594 Default settings in Comet were used with the following exceptions according to the MS/MS  
595 data type. iTRAQ-4plex (PXD010776): decoy\_search = 1, peptide\_mass\_tolerance= 10.00,  
596 fragment\_bin\_tol = 0.1, fragment\_bin\_offset = 0.0, theoretical\_fragment\_ions = 0,  
597 spectrum\_batch\_size = 15000, clear\_mz\_range = 113.5-117.5, add\_Nterm\_peptide = 144.10253,  
598 add\_K\_lycine = 144.10253, minimum\_peaks = 8. Label-free (PXD014381): decoy\_search = 1,  
599 peptide\_mass\_tolerance = 10.00, fragment\_bin\_tol = 0.02, fragment\_bin\_offset = 0.0,  
600 theoretical\_fragment\_ions = 0, spectrum\_batch\_size = 15000.

601 CometUI (Eng et al., 2013) was employed for assessing Comet's \*.xml output files and setting  
602 a false discovery rate (FDR) threshold of 10% per peptide identification. This FDR threshold was  
603 selected due to expected low abundance levels of the target smORFs.

604

#### 605 **Conservation analysis**

606 Protein, cDNA and ncRNA sequence data for *H.sapiens*, *P.abelii*, *P.paniscus*, *P.troglodytes*,  
607 *G.gorilla*, *N.leucogenys*, and *M.musculus* were obtained from Ensembl (release 100, (Yates et al.,  
608 2020)).

609 A sequence homology search was performed using the 45 translated lncRNA peptide  
610 sequences, against each non-human species protein database using BLASTp (e value - 0.001) (Altschul

611 et al., 1990). As these are small peptides, results were filtered to remove anything with <75% identity,  
612 unless a result(s) was the lowest e value hit for a given query in each species. Results were returned  
613 for 12 lncRNA peptides, and manually cross validated using Ensembl Genome Browser and multiple  
614 sequence alignments performed using ClustalOmega (Sievers et al., 2011), run using default  
615 parameters using the msa package in R (Bodenhofer et al., 2015), to give 8 peptides with evidence of  
616 sequence conservation.

617 The transcript sequences of the 45 translated lncRNAs were searched against transcriptome  
618 databases created by combining the cDNA and ncRNA data for each species, using BLASTn (e value -  
619 0.001) (Altschul et al., 1990). Results of this BLAST were used to filter the initial BLAST databases. ORF  
620 portions of the 45 translated lncRNAs were extracted, and searched against these filtered databases  
621 using BLASTn (e value - 0.001)(Altschul et al., 1990).

622 It was confirmed that all the lncRNA ORFs returned their genes of origin in *H.sapiens*. The  
623 remaining species returned results for 18 of the lncRNA ORF queries. These were cross validated as  
624 above, resulting in 14 lncRNA ORFs with evidence of sequence conservation based on transcript  
625 sequences.

626 A final search was performed using the 45 translated lncRNA peptide sequences against the  
627 transcriptome databases using tBLASTn (e value - 0.001) (Altschul et al., 1990). To reduce redundancy,  
628 results were filtered to select the transcripts(s) with lowest e value for each gene. It was confirmed  
629 that all ORFs returned their genes of origin in *H.sapiens*.

630 The remaining species returned results for 21 of the lncRNA peptide queries. As some queries  
631 had many spurious results, they were further filtered to select the transcripts(s) with lowest e value  
632 for each query in each species. These were cross validated as above, resulting in 16 lncRNA peptides  
633 with evidence of sequence conservation based on transcript sequences.

634 We combined evidence from all these approaches into a final dataset consisting of 17 lncRNA  
635 small ORFs with evidence of conservation.

636

### 637 **Plasmid construction/Cloning**

638 5'-UTRs and CDSs of putative smORFs (lacking stop codon) were generated by PCR (Table 3),  
639 using NEB High Fidelity DNA Polymerase (Q5). C-terminal 3xFLAG tag was incorporated within the  
640 reverse primer (Table 3 marked with green) by PCR and products were cloned into NheI and EcoRV  
641 restriction sites (Table 3: marked with blue) of pcDNA3.1-hygro vector (Addgene, kindly provided by  
642 Mark Richards-Bayliss group, University of Leeds). Start codon mutations were generated by site  
643 directed mutagenesis (Q5 Site directed mutagenesis kit, NEB).

644

645 **Transfections and Microscopy**

646 Plasmid transfections were performed using Lipofectamine 3000 (Thermo) following the  
647 manufacturer's instructions. After 48 h, the cells were fixed for 20 min with 4% paraformaldehyde,  
648 washed with 1X PBS, 0.1% Triton X-100 (PBS-T) and processed for immunocytochemistry as previously  
649 described. Imaging was conducted using EVOS fluorescent microscope.

650

651 **siRNA knockdown**

652 siRNA knockdown was performed using Lincode siRNA SMARTpool (Dharmacon) (LINC01116  
653 transcript: R-027999-00-0005 SMARTpool). Lincode Non-targeting Pool (D-001810-10) was used as  
654 scrambled control. Cells were seeded in 24-well plates ( $10^5$  cells/well,) and siRNA where transfected  
655 using RNAiMAX lipofectamine (ThermoFisher) as per manufacturer's instructions.

656

657 **General statistics and plots**

658 Statistical analyses were performed in R (R Core Team, 2019), using packages including stringr  
659 (Wickham, 2019), dplyr (Wickham, 2017), tidyr (Wickham, 2017), protr (Xiao et al., 2015) ggplot  
660 (Wickham, 2016), ggstatsplot (Patil, 2018), knitr (Xie, 2020), seqinr (Charif D, 2007), ggbeeswarm  
661 (Clarke & Sherrill-Mix, 2017), and EnhancedVolcano (Blighe et al., 2018)

662 Experimental values from independent samples with equal variances, were assessed using 2-  
663 tailed unpaired Student's t-test. The results are shown as mean $\pm$ SEM values of 3 independent  
664 replicates. The exact P values are described and specified in each figure legend. P values  $< 0.05$  were  
665 considered statistically significant.

666

667 **Data availability**

668 Poly-Ribo-Seq datasets will be deposited in GEO.

669

670

671

672

673

674

675 **Tables**

676 **Table 1: Buffers**

<b>Polysome lysis buffer (1mL/70 million cells)</b>	
---	--

Component	final concentration
Tris-HCl pH8	50mM
NaCl	150mM
MgCl <sub>2</sub>	10mM
DTT	1mM
IGEPAL	1%
cycloheximide	100µg/mL
Turbo DNase	24U/mL
RNase Inhibitor (RNaseInPlus)	90U
Complete Protease Inhibitor (Roche)	0.33%
ddH <sub>2</sub> O	
<b>RNasel footprinting buffer</b>	
Component	final concentration
Tris-HCl pH8	100mM
NaCl	30mM
MgCl <sub>2</sub>	10mM
RNasel (EN0601-Thermo)	0.8-1U/million cells
SuperRNase Inhibitor (Ambion)	3U/million cells
<b>Cytoplasmic/Nuclear fractionation buffer</b>	
Component	final concentration
Phosphate Buffer Saline (PBS)	1X
Triton-X	1%
RNase Inhibitor (RNaseInPlus)	40U/mL
ddH <sub>2</sub> O	
<b>Nuclei lysis buffer-RIPA based</b>	
Component	final concentration
NaCl	150mM
IGEPAL	1%

Sodium Deoxycholate (DOC)	0.5%
SDS	0.1%
Tris-HCl pH 7.4	25mM
cOmplete Protease Inhibitor (Roche)	1X
ddH <sub>2</sub> O	

677

678

679

680 Table 2: qPCR primers

qPCR		
gene/transcript	Forward primer sequence	Reverse primer sequence
MOXD1	GGAAGCCGAAAAGCCAAGTG	TCGAAAATGACGCAGCCTGA
NTN4	CGAGTGCAGAACCTGCAAGTGT	CATCTGGAGCTGAGAAGGGTC
E2F1	TGGAGCAAGAACCGCTGTTGT	GGGAAAGGCTGATGAACCTCCT
SOX2	ACATGAACGGCTGGAGCAA	GTAAGACATGCTGTAGGTGGG
GAPDH	CATCCTGGGCTACACTGAGC	GTCAAAGGTGGAGGAGTGGG
LINC01116	TCTAAGAATGGGCTCACTCTGC	CCAGGCATGGTGGCTCAC
LINC02143	AACCTTGCAGTAGCTCCTGG	GGATGAGGAGACTGAGACTGAGAG
AC254633.1	GTGACTCACCTCCCAGACTTC	TGCTGTGCAGCCAGCGTC
DLGAP1-AS1	TCTGAGAGCCAGCGAACTTT	AGCCTGTTGCGTCATGTGAT
DLGAP1-AS2	CCCAGGACACAGACAAGACC	ATGCACGCTCTGACAGCA
SERPINB9P1	AGTCAGCGAGTGGACAAAGC	GACTCCATGCTGCGGTTTC
AC090001.1	GTGCCCATGAGGGAGAACAC	GACAAGAAGTCAGGAGGTAGACA
SNAP25-AS1	AGCCATGGAAGTCAAATGCTG	AGGCATTTGCTGTCTTCCTC
XIST	GGCTCCTCTGGACATTCTGAG	AGCTTGGCCAGATTCTCAAAG

681

682

683

684

685 Table 3: Cloning Primers

Transcript	Forward primer sequence	Reverse primer sequence
LINC001116-smORF	GGCGGT <b>GCTAGC</b> GCGAGCCACGGGCCTC	GGCGGT <b>GATATC</b> TCACTTGTACCGTCATCCTGTAATCGATGTCATGATCTTATAATCACCGTCATGGCTTTGAGTCGTTTTAAGCTGACTTGT
LINC01116-whole	GGCGGT <b>GCTAGC</b> GCGAGCCACGGGCCTC	ACCGCC <b>GATATC</b> CAATTACTGCATTACGTATTCTTC
LINC00478	GGCGGT <b>GCTAGC</b> CCTCCCTGTCGTTAACGATAAAATTCTCCA	GGCGGT <b>GATATC</b> TCACTTGTACCGTCATCCTGTAATCGATGTCATGATCTTATAATCACCGTCATGGCTTTGAGTCGTTAGTAAATGCTCTGA
LINC01116-mutant (ATG1)	CTTCTAAGAAAAGGTCTCACTCTGC	CAATTCAAGTTGTCTTCTAATAC
LINC01116-mutant (ATG2)	GGCACCATCAAAGCTCACTGCAGC	ACCACACTCCAGCCTGGG
LINC01116-mutant (both ATG)	GCTGGAGTGTGGTGGCACCATCAAAGCTCACTGCAGCCTGA A	CTGGGTGATGGCAGAGTGAGACCTTTCTAGAAGCAATTCAAGTTGTC

686

687

688

689

690

691

692

693

694

695

696

697

698 Table 4: Antibodies

Protein	Species	Company	Usage (ICC/WB)	Dilution
betaIII-tubulin (TuJ1)	rabbit	ProteinTech	ICC	1:50
ki67	mouse	Dako-Agilent	ICC	1:100
c-Fos	rabbit	Santa Cruz	ICC	1:50
Tubulin B	mouse	DSHB	both	1:5000 for WB, 1:200 for ICC
NXF1	mouse	abcam	WB	1:5000
H3K27me3	mouse	abcam	WB	1:1000
FLAG	mouse	Sigma	both	1:1000
hnRNPK	rabbit	abcam	ICC	1:100
anti-mouse IgG-HRP	goat	New England Biolabs	WB	1:5000
anti-rabbit IgG-HRP	goat	New England Biolabs	WB	1:5000
Alexa anti-mouse IgG-488	goat	Thermofisher	ICC	1:500
Alexa anti-rabbit IgG-488	goat	Thermofisher	ICC	1:500
Alexa anti-rabbit 633	goat	Thermofisher	ICC	1:500

699

700

701

702 **Acknowledgements**

703 We wish to thank Dr Eric Hewitt for providing the SH-SY5Y cells; Dr Iosifina Sampson and Dr Mark  
704 Richards (Bayliss group) for providing HEK293 cells and mammalian vectors. We thank the Next  
705 Generation Sequencing facility, at St James University Hospital, Leeds, UK for performing Next  
706 Generation Sequencing and Imaging Facility, Faculty of Biological Sciences, University of Leeds, UK  
707 for their assistance in confocal microscopy. Parts of this work were undertaken on ARC3, part of the  
708 High Performance Computing facilities at the University of Leeds, UK.

709

710 **Author contributions**

711 KD designed and performed experiments, acquired, analysed and interpreted data, drafted and  
712 revised the manuscript. IB designed and performed experiments, acquired, analysed and interpreted  
713 data, drafted and revised the manuscript. DW analysed, interpreted data and revised the  
714 manuscript. SC acquired and analysed data, and revised the manuscript. AB acquired and analysed  
715 data, and revised the manuscript. EJRV analysed data and revised the manuscript. MOC helped  
716 interpret portions of the data and critique the output for important intellectual content, and revised

717 the manuscript. JD helped design experiments, interpret portions of the data and critique the output  
718 for important intellectual content, and revised the manuscript. AW helped design experiments,  
719 interpret portions of the data and critique the output for important intellectual content, and revised  
720 the manuscript. JLA conceived the work, interpreted data, drafted and revised the manuscript.  
721

722 **Funding**

723 Katerina Douka's PhD was funded by Leeds Anniversary Research Scholarship (LARS). Julie Aspden is  
724 funded by the University of Leeds (University Academic Fellow scheme). This work was funded by  
725 MRC (MR/N000471/1).

726  
727

728 References

729

- 730 Altschul, S. F., Gish, W., Miller, W., Myers, E. W., & Lipman, D. J. (1990). BASIC LOCAL  
731 ALIGNMENT SEARCH TOOL [Article]. *Journal of Molecular Biology*, 215(3), 403-410.  
732 [https://doi.org/10.1016/s0022-2836\(05\)80360-2](https://doi.org/10.1016/s0022-2836(05)80360-2)
- 733 Anderson, D. M., Anderson, K. M., Chang, C. L., Makarewich, C. A., Nelson, B. R., McAnally, J.  
734 R., Kasaragod, P., Shelton, J. M., Liou, J., Bassel-Duby, R., & Olson, E. N. (2015). A  
735 micropeptide encoded by a putative long noncoding RNA regulates muscle  
736 performance. *Cell*, 160(4), 595-606.
- 737 Andrews, S. (2010). *FastQC: a quality control tool for high throughput sequence data*. In  
738 (Version v.0.11.8)
- 739 Aspden, J. L., Eyre-Walker, Y. C., Phillips, R. J., Amin, U., Mumtaz, M. A., Brocard, M., &  
740 Couso, J. P. (2014). Extensive translation of small Open Reading Frames revealed by  
741 Poly-Ribo-Seq. *eLife*, 3, e03528. <https://doi.org/10.7554/eLife.03528>
- 742 Bateman, A., Martin, M. J., Orchard, S., Magrane, M., Alpi, E., Bely, B., Bingley, M., Britto, R.,  
743 Bursteinas, B., Busiello, G., Bye-A-Jee, H., Da Silva, A., De Giorgi, M., Dogan, T.,  
744 Castro, L. G., Garmiri, P., Georghiou, G., Gonzales, D., Gonzales, L., Hatton-Ellis, E.,  
745 Ignatchenko, A., Ishtiaq, R., Jokinen, P., Joshi, V., Jyothi, D., Lopez, R., Luo, J., Lussi, Y.,  
746 MacDougall, A., Madeira, F., Mahmoudy, M., Menchi, M., Nightingale, A., Onwubiko,  
747 J., Palka, B., Pichler, K., Pundir, S., Qi, G. Y., Raj, S., Renaux, A., Lopez, M. R., Saidi, R.,  
748 Sawford, T., Shypitsyna, A., Speretta, E., Turner, E., Tyagi, N., Vasudev, P., Volynkin,  
749 V., Wardell, T., Warner, K., Watkins, X., Zaru, R., Zellner, H., Bridge, A., Xenarios, I.,  
750 Pou, S., Redaschi, N., Aimo, L., Argoud-Puy, G., Auchincloss, A., Axelsen, K., Bansal,  
751 P., Baratin, D., Blatter, M. C., Bolleman, J., Boutet, E., Breuza, L., Casals-Casas, C., de  
752 Castro, E., Coudert, E., Cuche, B., Doche, M., Dornevil, D., Estreicher, A., Famiglietti,  
753 L., Feuermann, M., Gasteiger, E., Gehant, S., Gerritsen, V., Gos, A., Gruaz, N., Hinz,  
754 U., Hulo, C., Hyka-Nouspikel, N., Jungo, F., Keller, G., Kerhornou, A., Lara, V.,  
755 Lemercier, P., Lieberherr, D., Lombardot, T., Martin, X., Masson, P., Morgat, A., Neto,  
756 T. B., Paesano, S., Pedruzzi, I., Pilbout, S., Pozzato, M., Pruess, M., Rivoire, C., Sigrist,  
757 C., Sonesson, K., Stutz, A., Sundaram, S., Tognolli, M., Verbregue, L., Wu, C. H., Arighi,  
758 C. N., Arminski, L., Chen, C. M., Chen, Y. X., Cowart, J., Garavelli, J. S., Huang, H. Z.,

- 759 Laiho, K., McGarvey, P., Natale, D. A., Ross, K., Vinayaka, C. R., Wang, Q. H., Wang, Y.  
760 Q., Yeh, L. S., Zhang, J., & UniProt, C. (2019). UniProt: a worldwide hub of protein  
761 knowledge [Article]. *Nucleic Acids Research*, 47(D1), D506-D515.  
<https://doi.org/10.1093/nar/gky1049>
- 762 Bazzini, A. A., Johnstone, T. G., Christiano, R., Mackowiak, S. D., Obermayer, B., Fleming, E.  
763 S., Vejnar, C. E., Lee, M. T., Rajewsky, N., Walther, T. C., & Giraldez, A. J. (2014).  
764 Identification of small ORFs in vertebrates using ribosome footprinting and  
765 evolutionary conservation. *EMBO J*, 33(9), 981-993.  
<https://doi.org/10.1002/embj.201488411>
- 766 Beckedorff, F. C., Ayupe, A. C., Crocci-Souza, R., Amaral, M. S., Nakaya, H. I., Soltys, D. T.,  
767 Menck, C. F., Reis, E. M., & Verjovski-Almeida, S. (2013). The intronic long noncoding  
768 RNA ANRASSF1 recruits PRC2 to the RASSF1A promoter, reducing the expression of  
769 RASSF1A and increasing cell proliferation. *PLoS Genet*, 9(8), e1003705.  
<https://doi.org/10.1371/journal.pgen.1003705>
- 770 Blair, J. D., Hockemeyer, D., Doudna, J. A., Bateup, H. S., & Floor, S. N. (2017). Widespread  
771 Translational Remodeling during Human Neuronal Differentiation. *Cell Reports*,  
772 21(7), 2005-2016. <https://doi.org/10.1016/j.celrep.2017.10.095>
- 773 Blighe, K., S, Rana, M., & Lewis. (2018). EnhancedVolcano: Publication-ready volcano plots  
774 with enhanced colouring and labeling. In  
775 Bodenhofer, U., Bonatesta, E., Horejs-Kainrath, C., & Hochreiter, S. (2015). msa: an R  
776 package for multiple sequence alignment [Article]. *Bioinformatics*, 31(24), 3997-  
777 3999. <https://doi.org/10.1093/bioinformatics/btv494>
- 778 Brenig, K., Grube, L., Schwarzländer, M., Köhrer, K., Stühler, K., & Poschmann, G. (2020). The  
779 Proteomic Landscape of Cysteine Oxidation That Underpins Retinoic Acid-Induced  
780 Neuronal Differentiation. *J Proteome Res*, 19(5), 1923-1940.  
<https://doi.org/10.1021/acs.jproteome.9b00752>
- 781 Brockdorff, N. (2018). Local Tandem Repeat Expansion in Xist RNA as a Model for the  
782 Functionalisation of ncRNA. *Non-Coding RNA*, 4(4), 28.
- 783 Brodie, S., Lee, H. K., Jiang, W., Cazacu, S., Xiang, C., Poisson, L. M., Datta, I., Kalkanis, S.,  
784 Ginsberg, D., & Brodie, C. (2017). The novel long non-coding RNA TALNEC2, regulates  
785 tumor cell growth and the stemness and radiation response of glioma stem cells.  
786 *Oncotarget*, 8(19), 31785--31801. <https://doi.org/10.18632/oncotarget.15991>
- 787 Calviello, L., Mukherjee, N., Wyler, E., Zauber, H., Hirsekorn, A., Selbach, M., Landthaler, M.,  
788 Obermayer, B., & Ohler, U. (2016). Detecting actively translated open reading frames  
789 in ribosome profiling data [Article]. *Nature Methods*, 13(2), 165-+.  
<https://doi.org/10.1038/nmeth.3688>
- 790 Carelli, S., Giallongo, T., Rey, F., Latorre, E., Bordoni, M., Mazzucchelli, S., Gorio, M. C.,  
791 Pansarasa, O., Provenzani, A., & Cereda, C. (2019). HuR interacts with lincBRN1a and  
792 lincBRN1b during neuronal stem cells differentiation. *RNA Biology*, 16(10), 1471--  
793 1485. <https://doi.org/10.1080/15476286.2019.1637698>
- 794 Carlevaro-Fita, J., Rahim, A., Guigó, R., Vardy, L. A., & Johnson, R. (2016). Cytoplasmic long  
795 noncoding RNAs are frequently bound to and degraded at ribosomes in human cells.  
796 *Rna*, 22(6), 867--882. <https://doi.org/10.1261/rna.053561.115>
- 797 Carrieri, C., Cimatti, L., Biagioli, M., Beugnet, A., Zucchelli, S., Fedele, S., Pesce, E., Ferrer, I.,  
798 Collavin, L., Santoro, C., Forrest, A. R. R., Piero, C., Biffo, S., Stupka, E., & Gustincich,  
799 S. (2012). Long non-coding antisense RNA controls Uchl1 translation through an

- 805 embedded SINEB2 repeat. *Nature*, 491(7424), 454--457.  
806 <https://doi.org/10.1038/nature11508>
- 807 Carén, H., Ejeskär, K., Fransson, S., Hesson, L., Latif, F., Sjöberg, R. M., Krona, C., &  
808 Martinsson, T. (2005). A cluster of genes located in 1p36 are down-regulated in  
809 neuroblastomas with poor prognosis, but not due to CpG island methylation. *Mol  
810 Cancer*, 4(1), 10. <https://doi.org/10.1186/1476-4598-4-10>
- 811 Chan, P. P., & Lowe, T. M. (2016). GtRNAdb 2.0: an expanded database of transfer RNA  
812 genes identified in complete and draft genomes. *Nucleic Acids Research*, 44(D1),  
813 D184-D189. <https://doi.org/10.1093/nar/gkv1309>
- 814 Charif D, L. J. (2007). *SeqinR 1.0-2: a contributed package to the R project for statistical  
815 computing devoted to biological sequences retrieval and analysis*. In  
816 Chau, K. F., Shannon, M. L., Fame, R. M., Fonseca, E., Mullan, H., Johnson, M. B.,  
817 Sendamarai, A. K., Springel, M. W., Laurent, B., & Lehtinen, M. K. (2018).  
818 Downregulation of ribosome biogenesis during early forebrain development. *Elife*, 7.
- 819 Chen, J., Brunner, A.-D., Cogan, J. Z., Nuez, J. K., Fields, A. P., Adamson, B., Itzhak, D. N., Li, J.  
820 Y., Mann, M., Leonetti, M. D., & Weissman, J. S. (2020). Pervasive functional  
821 translation of noncanonical human open reading frames. *Science*, 367(6482), 1140--  
822 1146. <https://doi.org/10.1126/science.aay0262>
- 823 Chodroff, R. A., Goodstadt, L., Sirey, T. M., Oliver, P. L., Davies, K. E., Green, E. D., Molnár, Z.,  
824 & Ponting, C. P. (2010). Long noncoding RNA genes: conservation of sequence and  
825 brain expression among diverse amniotes.
- 826 Chong, C., Müller, M., Pak, H., Harnett, D., Huber, F., Grun, D., Leleu, M., Auger, A., Arnaud,  
827 M., Stevenson, B. J., Michaux, J., Bilic, I., Hirsekorn, A., Calviello, L., Simó-Riudalbas,  
828 L., Planet, E., Lubiński, J., Bryśkiewicz, M., Wiznerowicz, M., Xenarios, I., Zhang, L.,  
829 Trono, D., Harari, A., Ohler, U., Coukos, G., & Bassani-Sternberg, M. (2020).  
830 Integrated proteogenomic deep sequencing and analytics accurately identify non-  
831 canonical peptides in tumor immunopeptidomes. *Nat Commun*, 11(1), 1293.
- 832 Chothani, S., Adami, E., Ouyang, J. F., Viswanathan, S., Hubner, N., Cook, S. A., Schafer, S., &  
833 Rackham, O. J. L. (2019). deltaTE: Detection of Translationally Regulated Genes by  
834 Integrative Analysis of Ribo-seq and RNA-seq Data. *Current Protocols in Molecular  
835 Biology*, 129(1), e108.
- 836 Clarke, E., & Sherrill-Mix, S. c. (2017). *ggbeeswarm: Categorical Scatter (Violin Point) Plots*.  
837 In <https://CRAN.R-project.org/package=ggbeeswarm>
- 838 Consortium, G. T. (2013). The Genotype-Tissue Expression (GTEx) project. *Nature Genetics*.  
839 <https://doi.org/10.1038/ng.2653>
- 840 Derrien, T., Johnson, R., Bussotti, G., Tanzer, A., Djebali, S., Tilgner, H., Guernec, G., Martin,  
841 D., Merkel, A., Knowles, D. G., Lagarde, J., Veeravalli, L., Ruan, X., Ruan, Y., Lassmann,  
842 T., Carninci, P., Brown, J. B., Lipovich, L., Gonzalez, J. M., Thomas, M., Davis, C. A.,  
843 Shiekhattar, R., Gingeras, T. R., Hubbard, T. J., Notredame, C., Harrow, J., & Guigó, R.  
844 (2012). The GENCODE v7 catalog of human long noncoding RNAs: analysis of their  
845 gene structure, evolution, and expression. *Genome Res*, 22(9), 1775-1789.
- 846 Dimartino, D., Colantoni, A., Ballarino, M., Martone, J., Mariani, D., Danner, J., Bruckmann,  
847 A., Meister, G., Morlando, M., & Bozzoni, I. (2018). The Long Non-coding RNA Inc-31  
848 Interacts with Rock1 mRNA and Mediates Its YB-1-Dependent Translation. *Cell  
849 Reports*, 23(3), 733--740. <https://doi.org/10.1016/j.celrep.2018.03.101>
- 850 Djebali, S., Davis, C. A., Merkel, A., Dobin, A., Lassmann, T., Mortazavi, A., Tanzer, A.,  
851 Lagarde, J., Lin, W., Schlesinger, F., Xue, C., Marinov, G. K., Khatun, J., Williams, B. A.,

- 852 Zaleski, C., Rozowsky, J., Röder, M., Kokocinski, F., Abdelhamid, R. F., Alioto, T.,  
853 Antoshechkin, I., Baer, M. T., Bar, N. S., Batut, P., Bell, K., Bell, I., Chakrabortty, S.,  
854 Chen, X., Chrast, J., Curado, J., Derrien, T., Drenkow, J., Dumais, E., Dumais, J.,  
855 Duttagupta, R., Falconnet, E., Fastuca, M., Fejes-Toth, K., Ferreira, P., Foissac, S.,  
856 Fullwood, M. J., Gao, H., Gonzalez, D., Gordon, A., Gunawardena, H., Howald, C., Jha,  
857 S., Johnson, R., Kapranov, P., King, B., Kingswood, C., Luo, O. J., Park, E., Persaud, K.,  
858 Preall, J. B., Ribeca, P., Risk, B., Robyr, D., Sammeth, M., Schaffer, L., See, L. H.,  
859 Shahab, A., Skancke, J., Suzuki, A. M., Takahashi, H., Tilgner, H., Trout, D., Walters,  
860 N., Wang, H., Wrobel, J., Yu, Y., Ruan, X., Hayashizaki, Y., Harrow, J., Gerstein, M.,  
861 Hubbard, T., Reymond, A., Antonarakis, S. E., Hannon, G., Giddings, M. C., Ruan, Y.,  
862 Wold, B., Carninci, P., Guigó, R., & Gingeras, T. R. (2012). Landscape of transcription  
863 in human cells. *Nature*, 489(7414), 101-108.
- 864 Dobin, A., Davis, C. A., Schlesinger, F., Drenkow, J., Zaleski, C., Jha, S., Batut, P., Chaisson, M.,  
865 & Gingeras, T. R. (2012). STAR: ultrafast universal RNA-seq aligner. *Bioinformatics*,  
866 29(1), 15-21. <https://doi.org/10.1093/bioinformatics/bts635>
- 867 Duncan, C. D. S., & Mata, J. (2014). The translational landscape of fission-yeast meiosis and  
868 sporulation. *Nature Structural & Molecular Biology*, 21(7), 641--647.  
869 <https://doi.org/10.1038/nsmb.2843>
- 870 Eden, E., Navon, R., Steinfeld, I., Lipson, D., & Yakhini, Z. (2009). GOrilla: a tool for discovery  
871 and visualization of enriched GO terms in ranked gene lists. *BMC Bioinformatics*,  
872 10(1), 48. <https://doi.org/10.1186/1471-2105-10-48>
- 873 Eng, J. K., Jahan, T. A., & Hoopmann, M. R. (2013). Comet: An open-source MS/MS sequence  
874 database search tool [Article]. *Proteomics*, 13(1), 22-24.  
875 <https://doi.org/10.1002/pmic.201200439>
- 876 Faghihi, M. A., Zhang, M., Huang, J., Modarresi, F., Van der Brug, M. P., Nalls, M. A.,  
877 Cookson, M. R., St-Laurent, G., 3rd, & Wahlestedt, C. (2010). Evidence for natural  
878 antisense transcript-mediated inhibition of microRNA function. *Genome Biol*, 11(5),  
879 R56.
- 880 Forster, J. I., Kglberger, S., Trefois, C., Boyd, O., Baumuratov, A. S., Buck, L., Balling, R., &  
881 Antony, P. M. A. (2016). Characterization of Differentiated SH-SY5Y as Neuronal  
882 Screening Model Reveals Increased Oxidative Vulnerability. *Journal of Biomolecular  
883 Screening*, 21(5), 496--509. <https://doi.org/10.1177/1087057115625190>
- 884 Frankish, A., Diekhans, M., Ferreira, A.-M., Johnson, R., Jungreis, I., Loveland, J., Mudge, J.  
885 M., Sisu, C., Wright, J., Armstrong, J., Barnes, I., Berry, A., Bignell, A., Carbonell Sala,  
886 S., Chrast, J., Cunningham, F., Di Domenico, T., Donaldson, S., Fiddes, I. T., García  
887 Girón, C., Gonzalez, J. M., Grego, T., Hardy, M., Hourlier, T., Hunt, T., Izuogu, O.,  
888 Lagarde, J., Martin, F. J., Martínez, L., Mohanan, S., Muir, P., Navarro, F. C. P., Parker,  
889 A., Pei, B., Pozo, F., Ruffier, M., Schmitt, B. M., Stapleton, E., Suner, M.-M., Sycheva,  
890 I., Uszczynska-Ratajczak, B., Xu, J., Yates, A., Zerbino, D., Zhang, Y., Aken, B.,  
891 Choudhary, J. S., Gerstein, M., Guigó, R., Hubbard, T. J. P., Kellis, M., Paten, B.,  
892 Reymond, A., Tress, M. L., & Flieck, P. (2019). GENCODE reference annotation for the  
893 human and mouse genomes. *Nucleic acids research*, 47(D1), D766--D773.  
894 <https://doi.org/10.1093/nar/gky955>
- 895 Fujii, K., Shi, Z., Zhulyn, O., Denans, N., & Barna, M. (2017). Pervasive translational regulation  
896 of the cell signalling circuitry underlies mammalian development. *Nature  
897 Communications*, 8(1), 14443. <https://doi.org/10.1038/ncomms14443>
- 898 Gordon, A. (2010). FASTQ/A short-reads pre-processing tools. In (Version v.0.0.14)

- 899 Guo, H., Ingolia, N. T., Weissman, J. S., & Bartel, D. P. (2010). Mammalian microRNAs  
900 predominantly act to decrease target mRNA levels. *Nature*, 466(7308), 835--840.  
901 <https://doi.org/10.1038/nature09267>
- 902 Guttman, M., Russell, P., Ingolia, N. T., Weissman, J. S., & Lander, E. S. (2013). Ribosome  
903 profiling provides evidence that large noncoding RNAs do not encode proteins. *Cell*,  
904 154(1), 240-251. <https://doi.org/10.1016/j.cell.2013.06.009>
- 905 Haeussler, M., Zweig, A. S., Tyner, C., Speir, M. L., Rosenbloom, K. R., Raney, B. J., Lee, C. M.,  
906 Lee, B. T., Hinrichs, A. S., Gonzalez, J. N., Gibson, D., Diekhans, M., Clawson, H.,  
907 Casper, J., Barber, G. P., Haussler, D., Kuhn, R. M., & Kent, W. J. (2019). The UCSC  
908 Genome Browser database: 2019 update. *Nucleic acids research*, 47(D1), D853--  
909 D858. <https://doi.org/10.1093/nar/gky1095>
- 910 Hannon, G. J. (2010). FASTX-Toolkit.
- 911 Hulstaert, N., Shofstahl, J., Sachsenberg, T., Walzer, M., Barsnes, H., Martens, L., & Perez-  
912 Riverol, Y. (2020). ThermoRawFileParser: Modular, Scalable, and Cross-Platform RAW  
913 File Conversion. *Journal of Proteome Research*, 19(1), 537-542.  
914 <https://doi.org/10.1021/acs.jproteome.9b00328>
- 915 Ingolia, N. T., Brar, G. A., Rouskin, S., McGeachy, A. M., & Weissman, J. S. (2013). Genome-  
916 Wide Annotation and Quantitation of Translation by Ribosome Profiling. 4.18.11--  
917 14.18.19. <https://doi.org/10.1002/0471142727.mb0418s103>
- 918 Johnsson, P., Lipovich, L., Grander, D., & Morris, K. V. (2014). Evolutionary conservation of  
919 long non-coding RNAs; sequence, structure, function [Review]. *Biochimica Et  
920 Biophysica Acta-General Subjects*, 1840(3), 1063-1071.  
921 <https://doi.org/10.1016/j.bbagen.2013.10.035>
- 922 King, J. L., & Jukes, T. H. (1969). NON-DARWINIAN EVOLUTION [Article]. *Science*, 164(3881),  
923 788-. <https://doi.org/10.1126/science.164.3881.788>
- 924 Korecka, J. A., van Kesteren, R. E., Blaas, E., Spitzer, S. O., Kamstra, J. H., Smit, A. B., Swaab,  
925 D. F., Verhaagen, J., & Bossers, K. (2013). Phenotypic Characterization of Retinoic  
926 Acid Differentiated SH-SY5Y Cells by Transcriptional Profiling. *PLoS ONE*, 8(5),  
927 e63862. <https://doi.org/10.1371/journal.pone.0063862>
- 928 Krona, C., Ejeskär, K., Carén, H., Abel, F., Sjöberg, R. M., & Martinsson, T. (2004). A novel  
929 1p36.2 located gene, APITD1, with tumour-suppressive properties and a putative  
930 p53-binding domain, shows low expression in neuroblastoma tumours. *Br J Cancer*,  
931 91(6), 1119-1130. <https://doi.org/10.1038/sj.bjc.6602083>
- 932 Ladoukakis, E., Pereira, V., Magny, E. G., Eyre-Walker, A., & Couso, J. P. (2011). Hundreds of  
933 putatively functional small open reading frames in Drosophila [Article]. *Genome  
934 Biology*, 12(11), 17, Article R118. <https://doi.org/10.1186/gb-2011-12-11-r118>
- 935 Langmead, B., & Salzberg, S. L. (2012). Fast gapped-read alignment with Bowtie 2. *Nature  
936 Methods*, 9(4), 357-U354. <https://doi.org/10.1038/nmeth.1923>
- 937 Lewandowski, J. P., Dumbović, G., Watson, A. R., Hwang, T., Jacobs-Palmer, E., Chang, N.,  
938 Much, C., Turner, K., Kirby, C., Schulz, J. F., Müller, C.-L., Rubinstein, N. D., Groff, A.  
939 F., Liapis, S. C., Gerhardinger, C., Hubner, N., van Heesch, S., Hoekstra, H. E.,  
940 Sauvageau, M., & Rinn, J. L. (2019). The *Tug1* Locus is Essential for Male  
941 Fertility. *bioRxiv*, 562066. <https://doi.org/10.1101/562066>
- 942 Li, H., Handsaker, B., Wysoker, A., Fennell, T., Ruan, J., Homer, N., Marth, G., Abecasis, G., &  
943 Durbin, R. (2009). The Sequence Alignment/Map format and SAMtools.  
944 *Bioinformatics (Oxford, England)*, 25(16), 2078--2079.  
945 <https://doi.org/10.1093/bioinformatics/btp352>

- 946 Liao, Y., Smyth, G. K., & Shi, W. (2013). The Subread aligner: fast, accurate and scalable read  
947 mapping by seed-and-vote. *Nucleic acids research*, 41(10), e108--e108.  
948 <https://doi.org/10.1093/nar/gkt214>
- 949 Liao, Y., Smyth, G. K., & Shi, W. (2014). featureCounts: an efficient general purpose program  
950 for assigning sequence reads to genomic features. *Bioinformatics (Oxford, England)*,  
951 30(7), 923--930. <https://doi.org/10.1093/bioinformatics/btt656>
- 952 Lin, N., Chang, K.-Y., Li, Z., Gates, K., Rana, Z. A., Dang, J., Zhang, D., Han, T., Yang, C.-S.,  
953 Cunningham, T. J., Head, S. R., Duester, G., Dong, P. D. S., & Rana, T. M. (2014). An  
954 Evolutionarily Conserved Long Noncoding RNA TUNA Controls Pluripotency and  
955 Neural Lineage Commitment. *Molecular Cell*, 53(6), 1005--1019.  
956 <https://doi.org/https://doi.org/10.1016/j.molcel.2014.01.021>
- 957 Lindsay, S. J., Xu, Y., Lisgo, S. N., Harkin, L. F., Copp, A. J., Gerrelli, D., Clownry, G. J., Talbot, A.,  
958 Keogh, M. J., Coxhead, J., Santibanez-Koref, M., & Chinnery, P. F. (2016). HDBR  
959 Expression: A Unique Resource for Global and Individual Gene Expression Studies  
960 during Early Human Brain Development. *Frontiers in Neuroanatomy*.  
961 <https://doi.org/10.3389/fnana.2016.00086>
- 962 Love, M. I., Huber, W., & Anders, S. (2014). Moderated estimation of fold change and  
963 dispersion for RNA-seq data with DESeq2. *Genome Biology*, 15(12), 550.  
964 <https://doi.org/10.1186/s13059-014-0550-8>
- 965 Maden, M. (2007). Retinoic acid in the development, regeneration and maintenance of the  
966 nervous system. *Nature Reviews Neuroscience*, 8(10), 755-765.  
967 <https://doi.org/10.1038/nrn2212>
- 968 Magny, E. G., Pueyo, J. I., Pearl, F. M., Cespedes, M. A., Niven, J. E., Bishop, S. A., & Couso, J.  
969 P. (2013). Conserved regulation of cardiac calcium uptake by peptides encoded in  
970 small open reading frames. In *Science* (Vol. 341, pp. 1116-1120).  
971 <https://doi.org/10.1126/science.1238802>
- 972 Martin, M. (2011). Cutadapt removes adapter sequences from high-throughput sequencing  
973 reads. 2011, 17(1), 3. <https://doi.org/10.14806/ej.17.1.200>
- 974 Michel, A. M., Mullan, J. P. A., Velayudhan, V., O'Connor, P. B. F., Donohue, C. A., & Baranov,  
975 P. V. (2016). RiboGalaxy: A browser based platform for the alignment, analysis and  
976 visualization of ribosome profiling data [Article]. *Rna Biology*, 13(3), 316-319.  
977 <https://doi.org/10.1080/15476286.2016.1141862>
- 978 Mohammad, L., Wiseman, J., Erickson, S., & Yang, G. (2019). Protein Synthesis and  
979 Translational Control in Neural Stem Cell Development and Neurogenesis.  
980 <https://doi.org/10.1093/oxfordhb/9780190686307.013.21>
- 981 Murillo, J. R., Pla, I., Goto-Silva, L., Nogueira, F. C. S., Domont, G. B., Perez-Riverol, Y.,  
982 Sánchez, A., & Junqueira, M. (2018). Mass spectrometry evaluation of a  
983 neuroblastoma SH-SY5Y cell culture protocol. *Anal Biochem*, 559, 51-54.  
984 <https://doi.org/10.1016/j.ab.2018.08.013>
- 985 Patil, I. (2018). *ggstatsplot: 'ggplot2' Based Plots with Statistical Details*. In <https://cran.r-project.org/web/packages/ggstatsplot/index.html>
- 986 Patraquim, P., Mumtaz, M. A. S., Pueyo, J. I., Aspden, J. L., & Couso, J. P. (2020).  
987 Developmental regulation of canonical and small ORF translation from mRNAs.  
988 *Genome Biol*, 21(1), 128. <https://doi.org/10.1186/s13059-020-02011-5>
- 989 Pedersen, A. G., & Nielsen, H. (1997). Neural network prediction of translation initiation  
990 sites in eukaryotes: perspectives for EST and genome analysis. *Proc Int Conf Intell  
991 Syst Mol Biol*, 5, 226-233.

- 993 Pollen, A. A., Nowakowski, T. J., Chen, J., Retallack, H., Sandoval-Espinosa, C., Nicholas, C. R.,  
994 Shuga, J., Liu, S. J., Oldham, M. C., Diaz, A., Lim, D. A., Leyrat, A. A., West, J. A., &  
995 Kriegstein, A. R. (2015). Molecular Identity of Human Outer Radial Glia during  
996 Cortical Development. *Cell*, 163(1), 55–67.  
997 <https://doi.org/10.1016/j.cell.2015.09.004>
- 998 Ponting, C. P., Oliver, P. L., & Reik, W. (2009). Evolution and Functions of Long Noncoding  
999 RNAs. *Cell*, 136(4), 629-641. <https://doi.org/10.1016/j.cell.2009.02.006>
- 1000 Pueyo, J. I., & Couso, J. P. (2008). The 11-aminoacid long Tarsal-less peptides trigger a cell  
1001 signal in Drosophila leg development. In *Dev Biol* (Vol. 324, pp. 192-201).  
1002 <https://doi.org/10.1016/j.ydbio.2008.08.025>
- 1003 Rodriguez, C. M., Chun, S. Y., Mills, R. E., & Todd, P. K. (2019). Translation of upstream open  
1004 reading frames in a model of neuronal differentiation. *BMC Genomics*, 20(1), 391.  
1005 <https://doi.org/10.1186/s12864-019-5775-1>
- 1006 Ruiz-Orera, J., & Alba, M. M. (2019). Conserved regions in long non-coding RNAs contain  
1007 abundant translation and protein–RNA interaction signatures. *NAR Genomics and*  
1008 *Bioinformatics*, 1(1), e2--e2. <https://doi.org/10.1093/nargab/lqz002>
- 1009 Saghatelian, A., & Couso, J. P. (2015). Discovery and characterization of smORF-encoded  
1010 bioactive polypeptides. *Nat Chem Biol*, 11(12), 909-916.  
1011 <https://doi.org/10.1038/nchembio.1964>
- 1012 Sievers, F., Wilm, A., Dineen, D., Gibson, T. J., Karplus, K., Li, W. Z., Lopez, R., McWilliam, H.,  
1013 Remmert, M., Soding, J., Thompson, J. D., & Higgins, D. G. (2011). Fast, scalable  
1014 generation of high-quality protein multiple sequence alignments using Clustal  
1015 Omega [Article]. *Molecular Systems Biology*, 7, 6, Article 539.  
1016 <https://doi.org/10.1038/msb.2011.75>
- 1017 Song, E. J., Werner, S. L., Neubauer, J., Stegmeier, F., Aspden, J., Rio, D., Harper, J. W.,  
1018 Elledge, S. J., Kirschner, M. W., & Rape, M. (2010). The Prp19 complex and the  
1019 Usp4Sart3 deubiquitinating enzyme control reversible ubiquitination at the  
1020 spliceosome. *Genes Dev*, 24(13), 1434-1447. <https://doi.org/10.1101/gad.1925010>
- 1021 Sossin, W. S., & Scheller, R. H. (1991). Biosynthesis and sorting of neuropeptides. *Curr Opin*  
1022 *Neurobiol*, 1(1), 79-83. [https://doi.org/10.1016/0959-4388\(91\)90013-w](https://doi.org/10.1016/0959-4388(91)90013-w)
- 1023 Spencer, H. L., Sanders, R., Boulberdaa, M., Meloni, M., Cochrane, A., Spiroski, A.-M.,  
1024 Mountford, J., Emanueli, C., Caporali, A., Brittan, M., Rodor, J., & Baker, A. H. (2020).  
1025 The LINC00961 transcript and its encoded micropeptide, small regulatory  
1026 polypeptide of amino acid response, regulate endothelial cell function.  
1027 *Cardiovascular Research*. <https://doi.org/10.1093/cvr/cvaa008>
- 1028 Su, X., Zhang, J., Luo, X., Yang, W., Liu, Y., Liu, Y., & Shan, Z. (2019). LncRNA LINC01116  
1029 Promotes Cancer Cell Proliferation, Migration And Invasion In Gastric Cancer By  
1030 Positively Interacting With lncRNA CASC11. *Oncotargets and Therapy*, Volume 12,  
1031 8117--8123. <https://doi.org/10.2147/OTT.S208133>
- 1032 Szafron, L. M., Balcerak, A., Grzybowska, E. A., Pienkowska-Grela, B., Felisiak-Golabek, A.,  
1033 Podgorska, A., Kulesza, M., Nowak, N., Pomorski, P., Wysocki, J., Rubel, T., Dansonka-  
1034 Mieszkowska, A., Konopka, B., Lukasik, M., & Kupryjanczyk, J. (2015). The Novel Gene  
1035 CRNDE Encodes a Nuclear Peptide (CRNDEP) Which Is Overexpressed in Highly  
1036 Proliferating Tissues. *PLoS one*, 10(5), e0127475-e0127475.  
1037 <https://doi.org/10.1371/journal.pone.0127475>

- 1038 Tsagakis, I., Douka, K., Birds, I., & Aspden, J. L. (2020). Long non-coding RNAs in  
1039 development and disease: Conservation to mechanisms. *J Pathol.*  
1040 <https://doi.org/10.1002/path.5405>
- 1041 van Heesch, S., Witte, F., Schneider-Lunitz, V., Schulz, J. F., Adami, E., Faber, A. B., Kirchner,  
1042 M., Maatz, H., Blachut, S., Sandmann, C. L., Kanda, M., Worth, C. L., Schafer, S.,  
1043 Calviello, L., Merriott, R., Patone, G., Hummel, O., Wyler, E., Obermayer, B., Mücke,  
1044 M. B., Lindberg, E. L., Trnka, F., Memczak, S., Schilling, M., Felkin, L. E., Barton, P. J.,  
1045 R., Quaife, N. M., Vanezis, K., Diecke, S., Mukai, M., Mah, N., Oh, S. J., Kurtz, A.,  
1046 Schramm, C., Schwinge, D., Sebode, M., Harakalova, M., Asselbergs, F. W., Vink, A.,  
1047 de Weger, R. A., Viswanathan, S., Widjaja, A. A., Gärtner-Rommel, A., Milting, H., Dos  
1048 Remedios, C., Knosalla, C., Mertins, P., Landthaler, M., Vingron, M., Linke, W. A.,  
1049 Seidman, J. G., Seidman, C. E., Rajewsky, N., Ohler, U., Cook, S. A., & Hubner, N.  
1050 (2019). The Translational Landscape of the Human Heart. In *Cell* (Vol. 178, pp. 242-  
1051 260 e229). © 2019 Elsevier Inc. <https://doi.org/10.1016/j.cell.2019.05.010>
- 1052 Wang, H., Iacoangeli, A., Popp, S., Muslimov, I. A., Hiroaki, I., Sonenberg, N., Lomakin, I. B., &  
1053 Tiedge, H. (2002). Dendritic BC1 RNA: Functional Role in Regulation of Translation  
1054 Initiation. *Journal of Neuroscience*, 22(23), 10232-10241.  
1055 <https://doi.org/10.1523/JNEUROSCI.22-23-10232.2002>
- 1056 Wang, L., Fan, J., Han, L., Qi, H., Wang, Y., Wang, H., Chen, S., Du, L., Li, S., Zhang, Y., Tang,  
1057 W., Ge, G., Pan, W., Hu, P., & Cheng, H. (2020). The micropeptide LEMP plays an  
1058 evolutionarily conserved role in myogenesis. *Cell Death & Disease*, 11(5), 357.  
1059 <https://doi.org/10.1038/s41419-020-2570-5>
- 1060 Wickham, H. (2019). *stringr: Simple, Consistent Wrappers for Common String Operations*. In  
1061 <https://CRAN.R-project.org/package=stringr>
- 1062 Winzi, M. a. (2018). The long noncoding RNA IncR492 inhibits neural differentiation of  
1063 murine embryonic stem cells. *Plos One*, 13(1), e0191682.  
1064 <https://doi.org/10.1371/journal.pone.0191682>
- 1065 Xiao, N., Cao, D. S., Zhu, M. F., & Xu, Q. S. (2015). protr/ProtrWeb: R package and web server  
1066 for generating various numerical representation schemes of protein sequences  
1067 [Article; Proceedings Paper]. *Bioinformatics*, 31(11), 1857-1859.  
1068 <https://doi.org/10.1093/bioinformatics/btv042>
- 1069 Xie, Y. (2020). *knitr: A General-Purpose Package for Dynamic Report Generation in R*. In  
1070 Xin, X., Mains, R. E., & Eipper, B. A. (2004). Monooxygenase X, a Member of the Copper-  
1071 dependent Monooxygenase Family Localized to the Endoplasmic Reticulum. *Journal  
1072 of Biological Chemistry*, 279(46), 48159-48167.  
1073 <https://doi.org/10.1074/jbc.M407486200>
- 1074 Yates, A. D., Achuthan, P., Akanni, W., Allen, J., Alvarez-Jarreta, J., Amode, M. R., Armean, I.  
1075 M., Azov, A. G., Bennett, R., Bhai, J., Billis, K., Boddu, S., Marugan, J. C., Cummins, C.,  
1076 Davidson, C., Dodiya, K., Fatima, R., Gall, A., Giron, C. G., Gil, L., Grego, T., Haggerty,  
1077 L., Haskell, E., Hourlier, T., Izuogu, O. G., Janacek, S. H., Juettemann, T., Kay, M.,  
1078 Lavidas, I., Le, T., Lemos, D., Martinez, J. G., Maurel, T., McDowall, M., McMahon, A.,  
1079 Mohanan, S., Moore, B., Nuhn, M., Oheh, D. N., Parker, A., Parton, A., Patricio, M.,  
1080 Sakthivel, M. P., Salam, A. I. A., Schmitt, B. M., Schuilenburg, H., Sheppard, D.,  
1081 Sycheva, M., Szuba, M., Taylor, K., Thormann, A., Threadgold, G., Vullo, A., Walts, B.,  
1082 Winterbottom, A., Zadissa, A., Chakiachvili, M., Flint, B., Frankish, A., Hunt, S. E.,  
1083 Ilsley, G., Kostadima, M., Langridge, N., Loveland, J. E., Martin, F. J., Morales, J.,  
1084 Mudge, J. M., Muffato, M., Perry, E., Ruffier, M., Trevanion, S. J., Cunningham, F.,

- 1085 Howe, K. L., Zerbino, D. R., & Flicek, P. (2020). Ensembl 2020 [Article]. *Nucleic Acids*  
1086 *Research*, 48(D1), D682-D688. <https://doi.org/10.1093/nar/gkz966>
- 1087 Zubarev, R. A. (2013). The challenge of the proteome dynamic range and its implications for  
1088 in-depth proteomics. *Proteomics*, 13(5), 723-726.  
1089 <https://doi.org/10.1002/pmic.201200451>
- 1090

# Figure 1

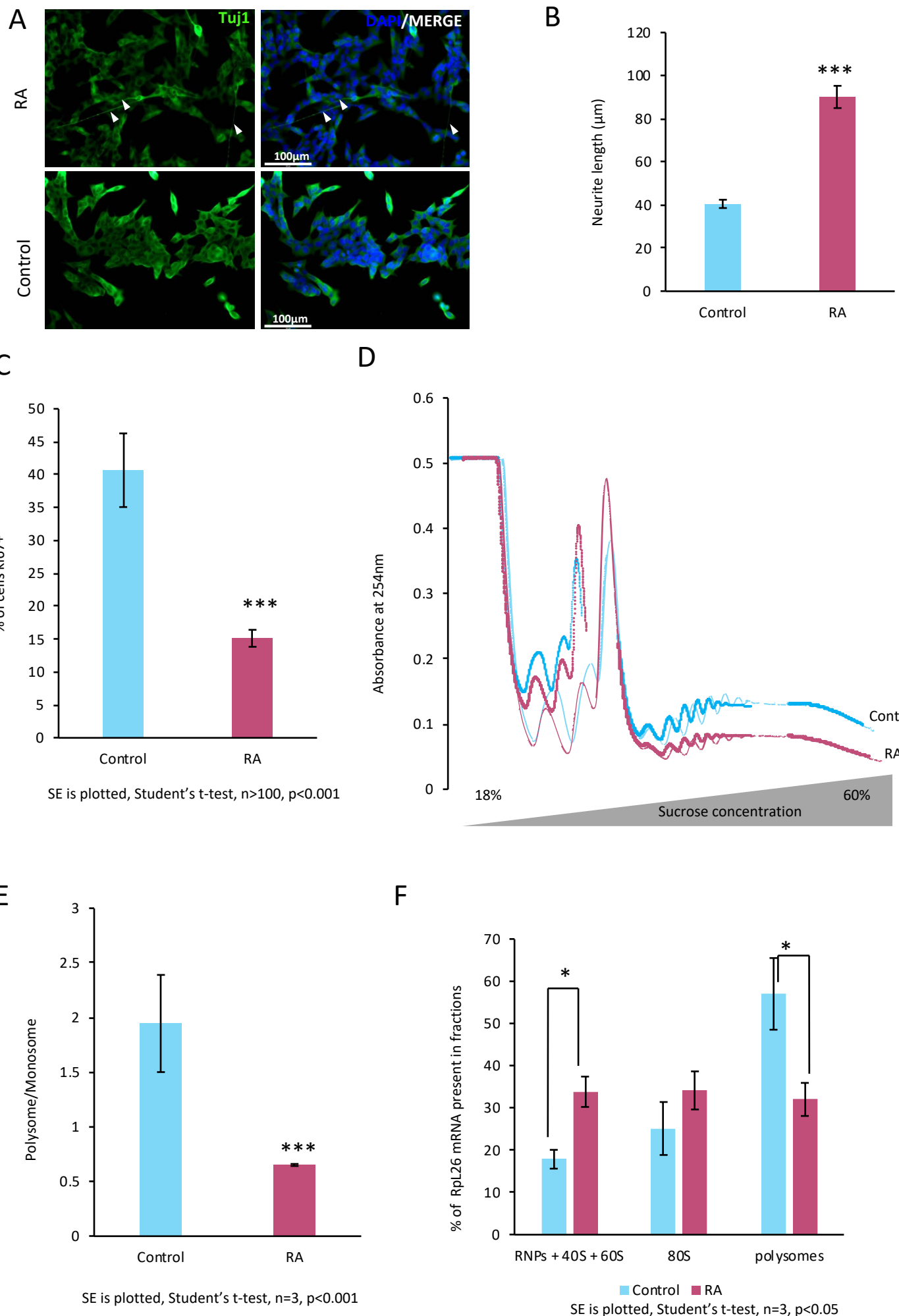
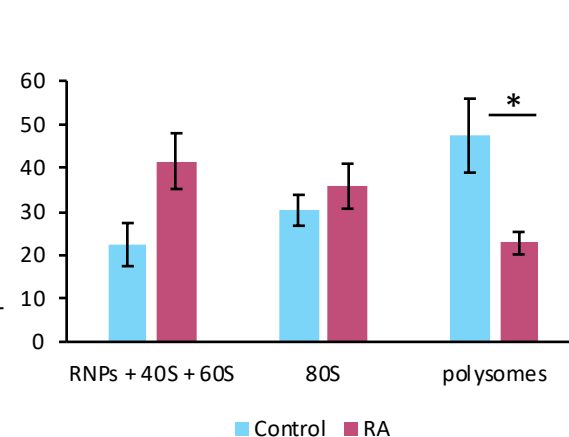
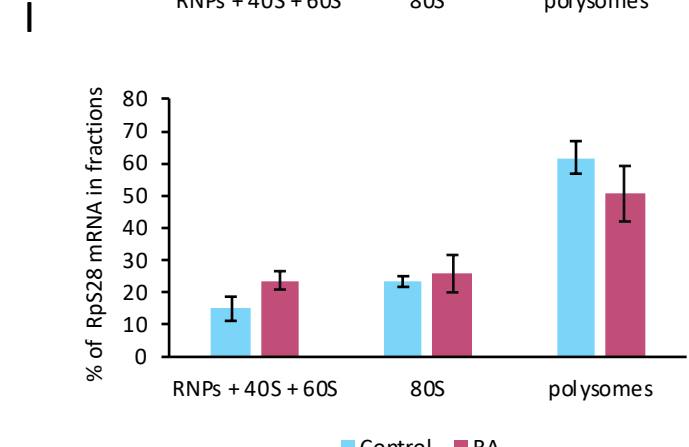
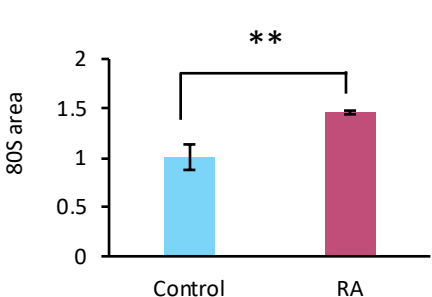
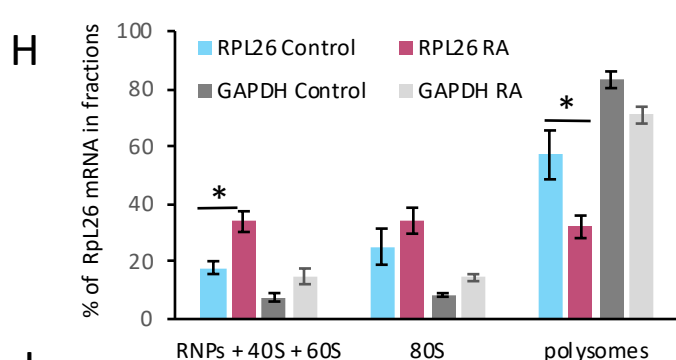
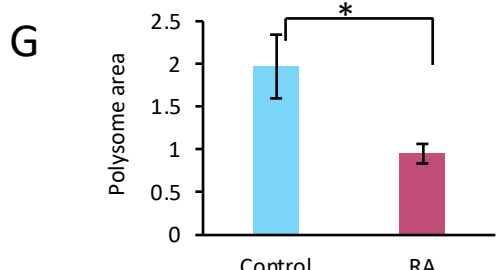
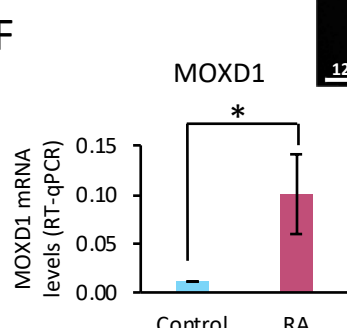
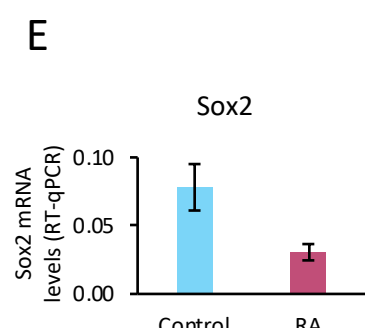
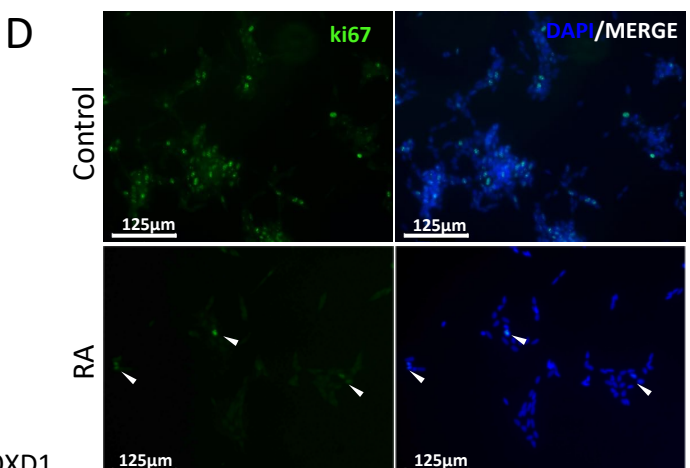
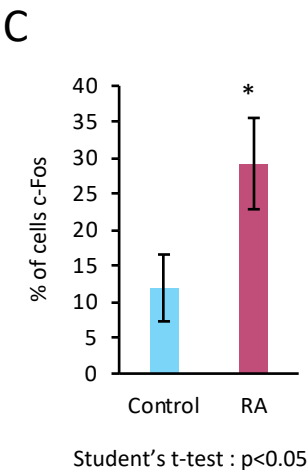
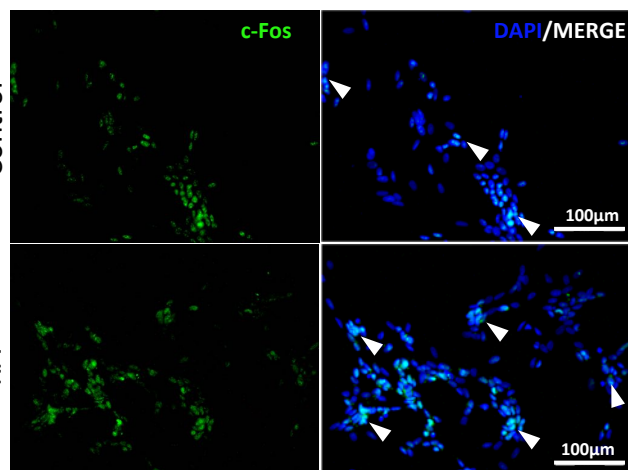
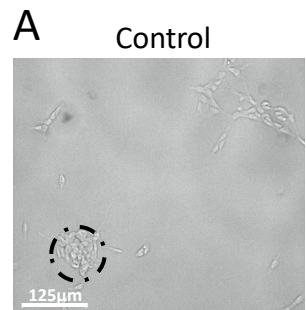


**Figure 1: Differentiation of SH-SY5Y results in a reduction in the level of active translation.**

Differentiation of SH-SY5Y cells with trans-retinoic acid (RA) for 3 days results in neurite elongation as seen by (A) representative immunofluorescence after staining for TuJ1 ( $\beta$ III-tubulin) (arrowheads mark elongated neurites) and (B) quantification of neurite length (Student's t-test, n=3, p<0.01). (C) RA treatment also results in reduction of proliferation, indicated by the reduction of ki67+ cells (Student's t-test, n=1000, p<0.001). (D) Sucrose gradient UV absorbance profiles of undifferentiated (Control) and differentiated (RA) cells reveals global translation is reduced upon differentiation. Peaks correspond to ribosomal subunits (40S, 60S), monosome (80S) and polysomes. (E) Quantification of Polysome/Monomosome (P/M) ratio indicates reduction of active translation is significant upon RA treatment (student's t-test, n=3, p<0.001). (F) RPL26 ribosomal protein mRNA shift from polysomes to RNPs and ribosomal subunits upon differentiation, as shown by RT-qPCR across gradient (student's t-test, n=3, p<0.05).

# Sup 1



Control RA

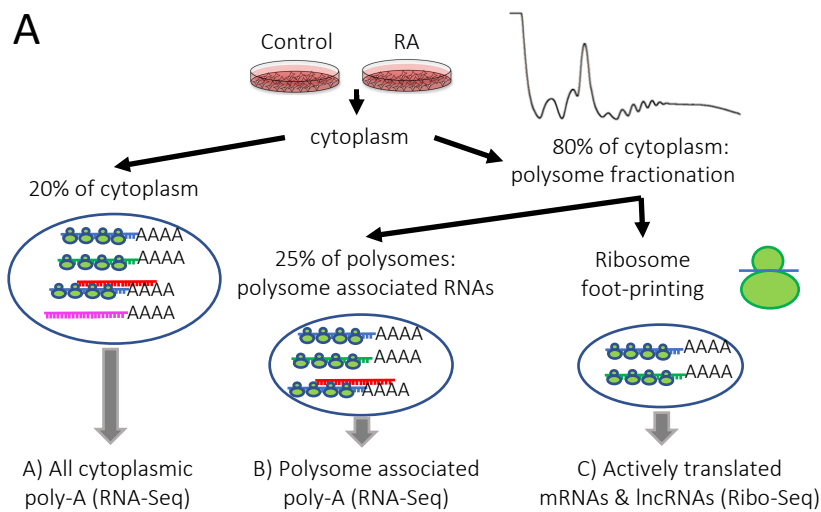
Control RA

### **Sup Figure 1: Differentiation of SH-SY5Y results in a reduction in the level of active translation.**

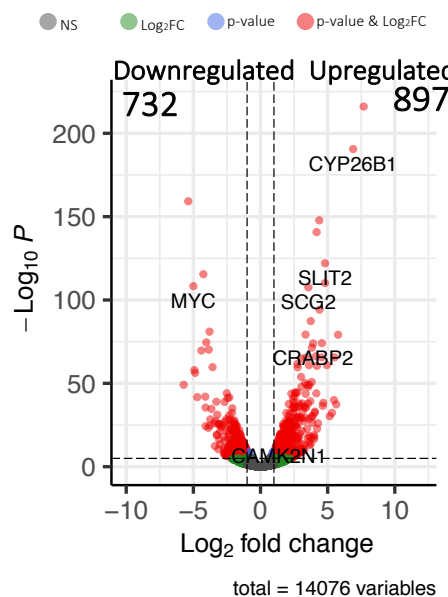
(A) Light microscopy reveals that undifferentiated SH-SY5Y cells grow in clumps and upon neural induction with RA they extend their neurites. (B) Immunofluorescence indicates c-Fos differentiation marker is expressed at higher levels in differentiated cells. (C) Quantification of c-Fos+ cells in Control and RA (Student's t-test, n=1000, p<0.05). (D) Immunofluorescence shows ki67 proliferation marker expression is reduced upon differentiation. (E) RT-qPCR of pluripotency/proliferation marker SOX2 shows reduced levels upon differentiation. (F) RT-qPCR of the differentiation marker MOXD1 indicates differentiation towards outer radial glia neural precursors (Student's t-test, n=3, p<0.05). (G) Quantification of polysome (Student's t-test, n=3, p<0.05) and monosome (Student's t-test, n=3, p<0.01) areas upon differentiation. (H) RT-qPCR of RPL26 mRNA distribution (Control; orange, RA; green) (with GAPDH mRNA controls; Control; light grey, RA; dark grey), in RNPs and ribosomal subunits (RNPs,40S, 60S), monosome (80S) and polysomes (Student's t-test, n=3, p<0.05). RT-qPCR across gradients of RPS28 (I) and RPL37 (J) mRNAs respectively (Student's t-test, n=3, p<0.05).

# Figure 2

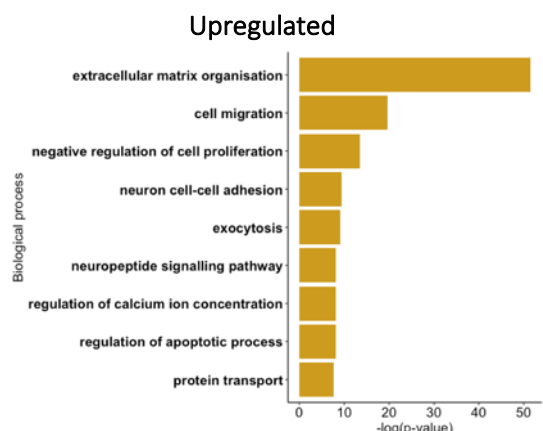
A



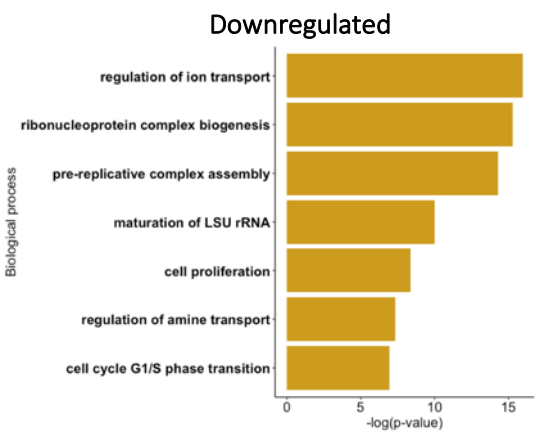
B



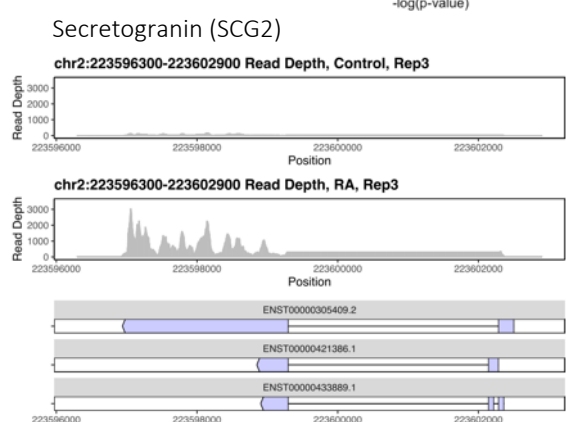
C



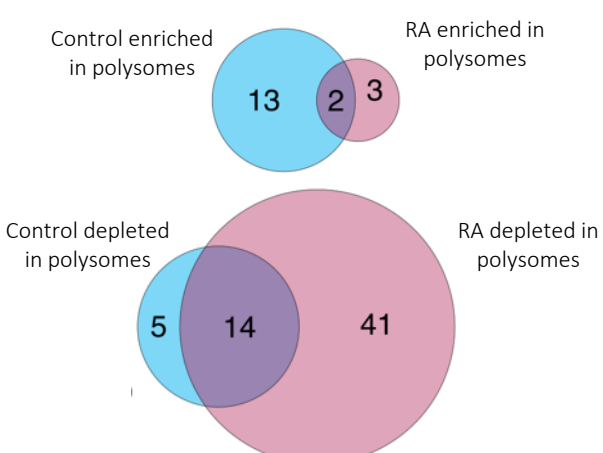
D



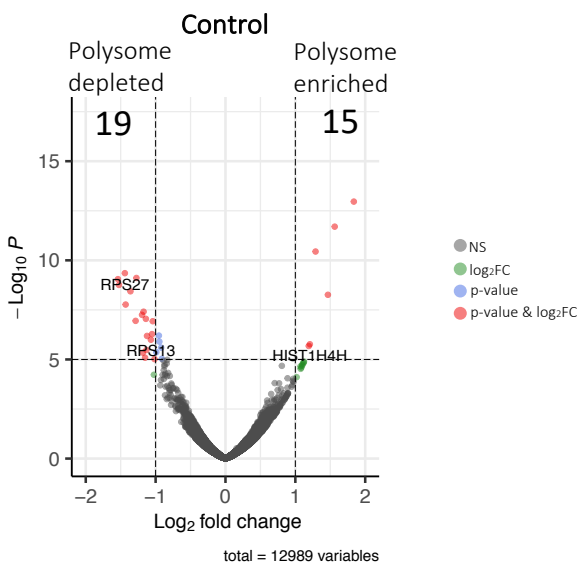
E



H



F



G

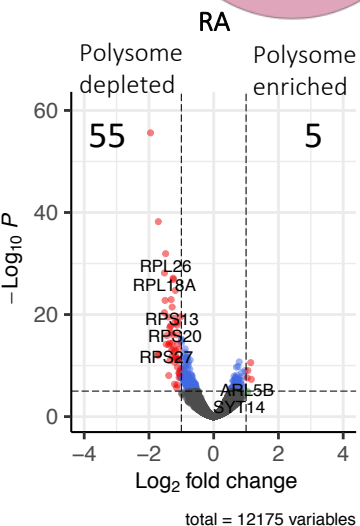
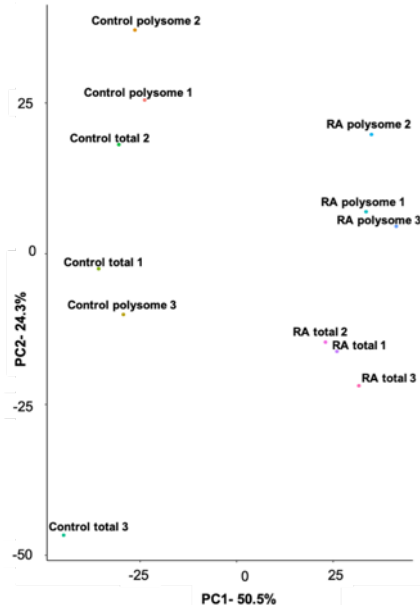


## Figure 2: Differentiation results in global RNA changes

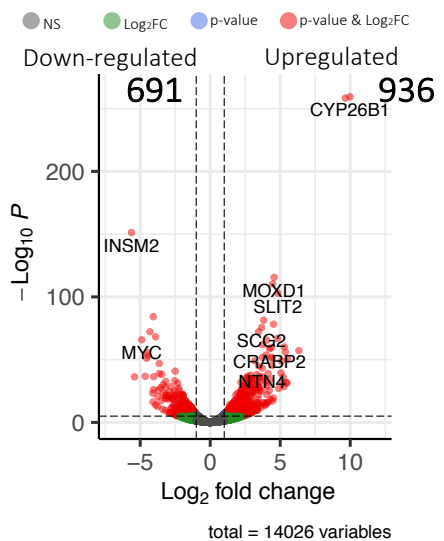
(A) Schematic of Poly-Ribo-Seq. (B) Volcano plot of protein-coding gene level changes in response to differentiation (polysome-associated); with 897 protein-coding genes significantly upregulated and 732 significantly downregulated ( $\log_2$  fold-change cut-off=1,  $p^{\text{adj}}<0.05$ ). GO terms enriched in polysome-associated protein-coding genes (C) upregulated and (D) downregulated upon differentiation. (E) Genome browser visualization of RNA-seq reads mapping to neuronal transcript Secretogranin, induced upon differentiation. (F, G) Volcano plots of differential expression of protein-coding transcripts between Total cytoplasm and polysomes for (F) Control and (G) RA, revealing the depletion of RP mRNAs from polysomes upon differentiation. (H) Venn diagrams of overlap between those mRNAs enriched or depleted in the polysomes between Control and RA.

# Sup 2

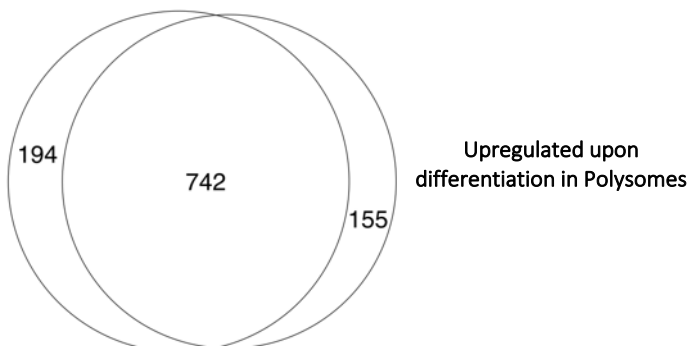
Control Total vs RA total



**B**



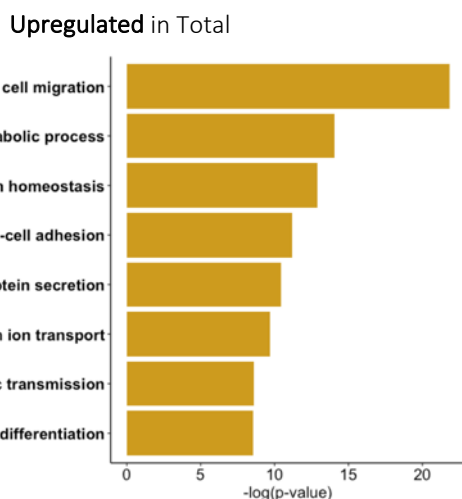
**C**



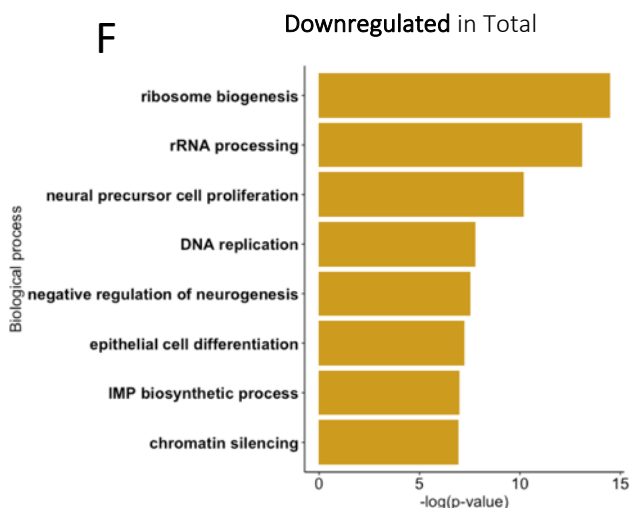
**D**



**E**



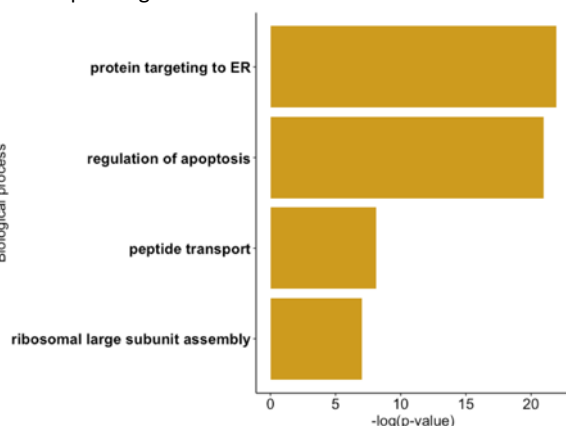
**F**



## Sup 2 cont

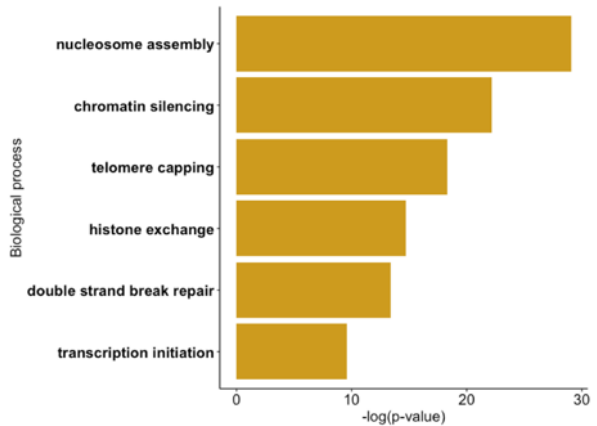
G

GO analysis of polysome depleted genes in Control

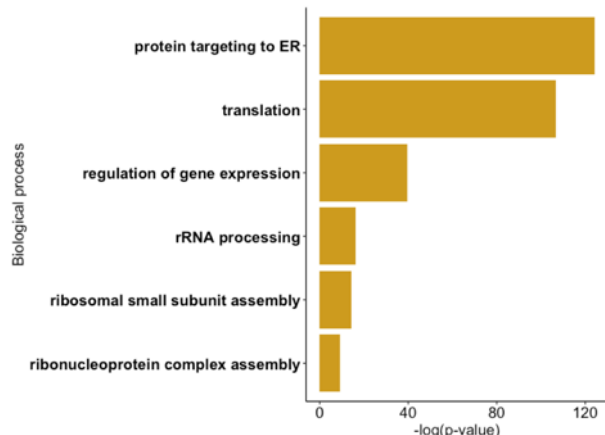


H

GO analysis of polysome enriched genes in Control



I GO analysis of polysome depleted genes in RA



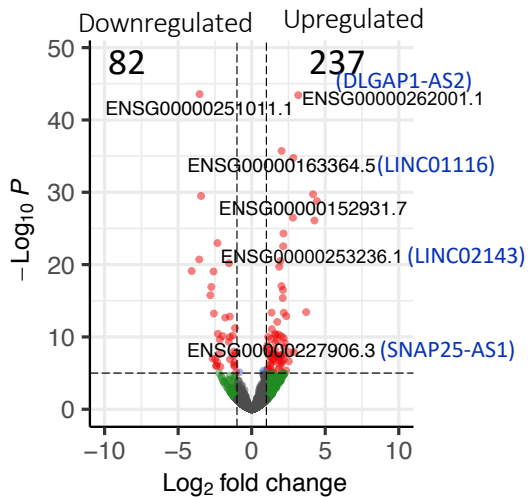
## Sup Figure 2: Differentiation results in global RNA changes

(A) PCA analysis of the RNA-Seq datasets shows that Control samples are more similar to each other than to RA treated samples. Control samples cluster separately from RA samples, indicating significant variation in gene expression between Control and differentiated cells. RA total samples cluster separately from RA polysome samples, whereas Control samples do not show different clustering, indicating that the variation in gene expression between RA total and RA polysome is greater than the variation between Control total and Control polysome. (B) Volcano plot depicting the differentially expressed protein-coding genes between Total Control and Total RA populations; 936 protein-coding mRNAs are upregulated and 691 downregulated upon differentiation ( $\log_2$  fold-change cut-off=1,  $p^{\text{adj}}<0.05$ ). Venn diagrams of overlap between those mRNAs identified as up (C) or down (D) regulated between Total and Polysome populations. GO term analysis for total cytoplasmic protein-coding genes (E) upregulated in and (F) downregulated. GO term analysis for protein-coding genes; (G) depleted from polysomes in Control, (H) enriched in polysomes in Control and (I) depleted from polysomes in RA.

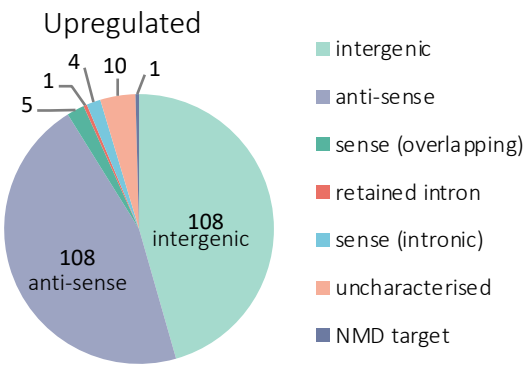
# Figure 3

Control vs RA Polysome associated lncRNAs

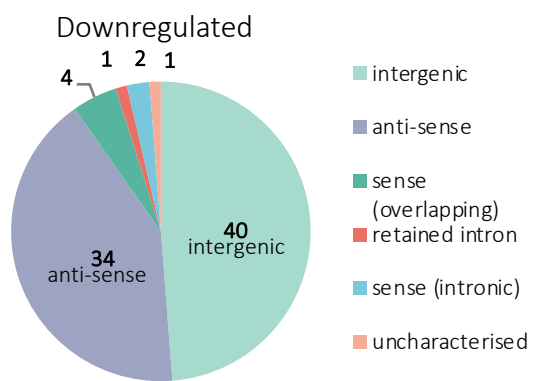
A



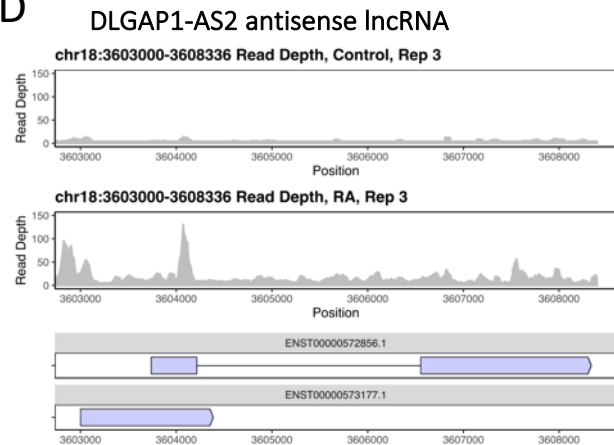
B



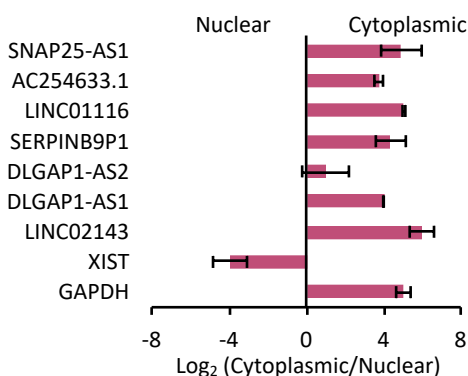
C



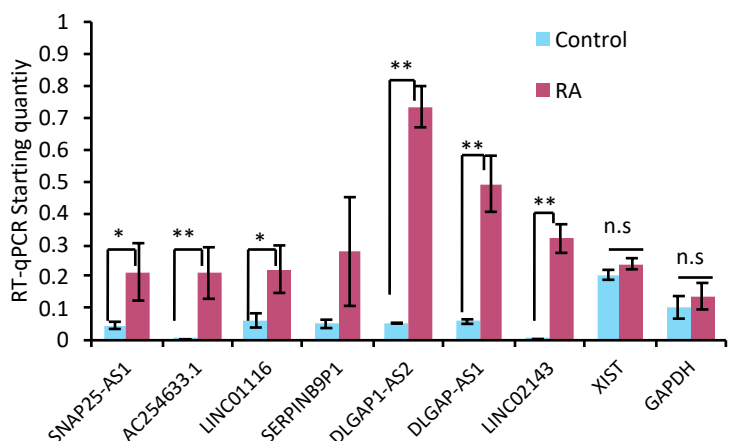
D



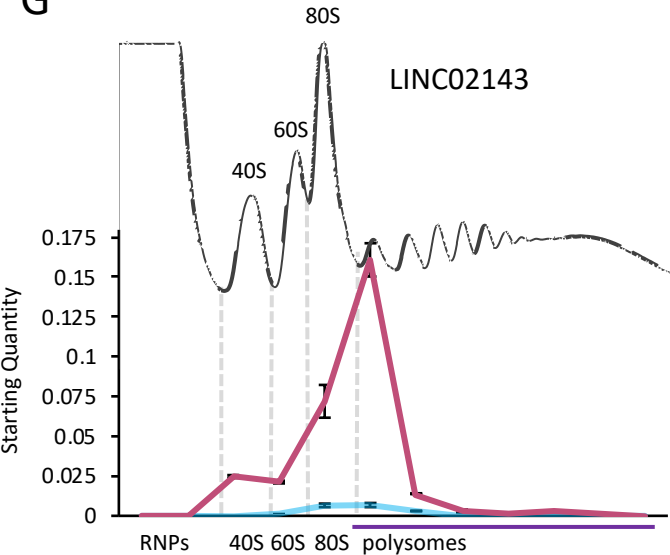
F



E



G



H

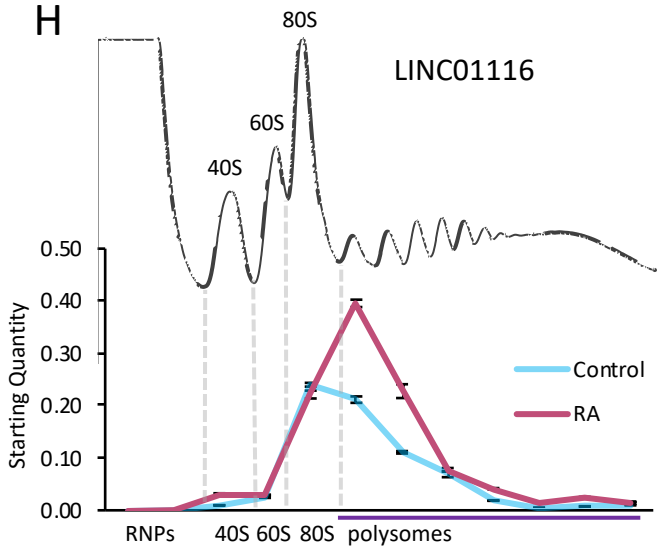
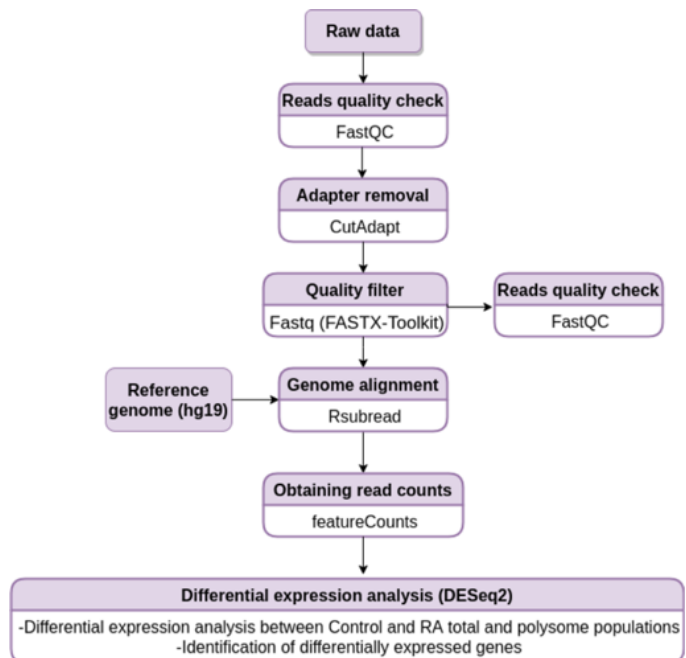


### Figure 3: LncRNAs regulated and associated with polysomes

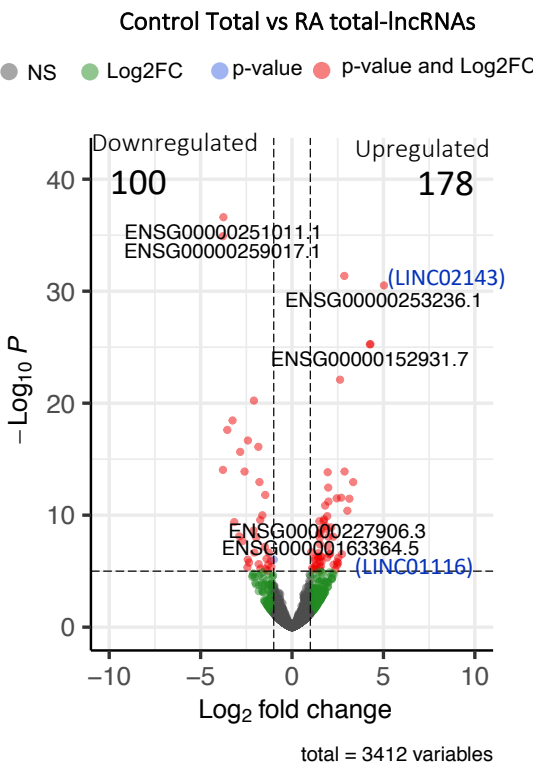
(A) Volcano plot displaying the differentially expressed polysome-associated lncRNAs (labelled by their geneIDs) between Control and RA populations. 237 lncRNAs are upregulated during differentiation and 82 downregulated ( $\log_2$  fold-change cutoff=1,  $p^{\text{adj}}<0.05$ ). Pie charts showing types of lncRNAs (B) upregulated and (C) downregulated upon differentiation (intergenic; anti-sense; sense-overlapping; retained intron; sense-intronic; uncharacterized; NMD target). (D) Example of lncRNA induced upon differentiation, DLGAP1-AS2. RNA-seq coverage for DLGAP1-AS2 in Control and RA conditions. (E) Changes in lncRNA levels upon differentiation validated by RT-qPCR, with XIST lncRNA and GAPDH mRNA as controls (SE is plotted,  $n=3$ , student's t-test  $p<0.05$  and  $p<0.01$ ). (F) lncRNAs of interest that are induced are specifically localised to cytoplasm as shown by subcellular fractionation RT-qPCR. XIST lncRNA was used as a nuclear and GAPDH mRNA as a cytoplasmic positive control ( $n=3$ , SE is plotted, student's t test,  $n=3$ ,  $p>0.05$ ). RT-qPCR of lncRNAs across sucrose gradient fractions indicates that (G) LINC02143 is found in 80S and small polysome fractions during differentiation (in differentiated cells 5% of the transcripts is detected in 80S (monosome) fraction and 65.6% in small polysome complexes) and (H) LINC01116 is found in 80S and 2-7 polysome fractions both in control and RA treated cells. On average, 66% of the LINC01116 transcripts is detected in the polysome fractions in Control and 57% upon differentiation. ( $n=3$ , SE is plotted).

# Sup 3

A

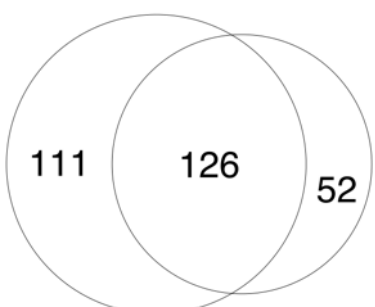


B



C

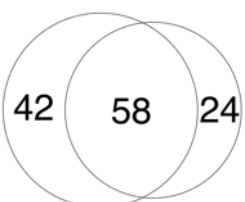
Upregulated lncRNAs upon differentiation in Total



Upregulated lncRNAs upon differentiation in Polysomes

D

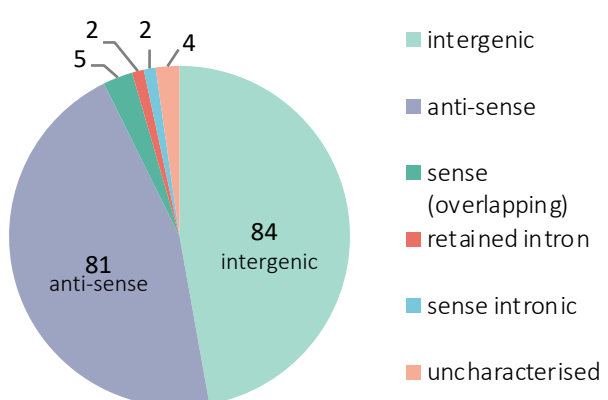
Downregulated lncRNAs upon differentiation in Total



Downregulated lncRNAs upon differentiation in Polysomes

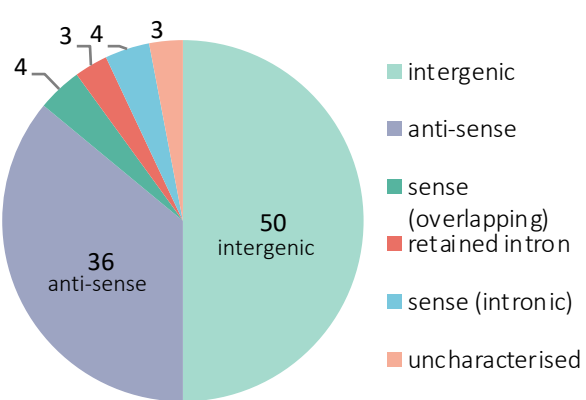
E

Upregulated lncRNAs upon differentiation in Total



F

Downregulated lncRNAs upon differentiation in Total

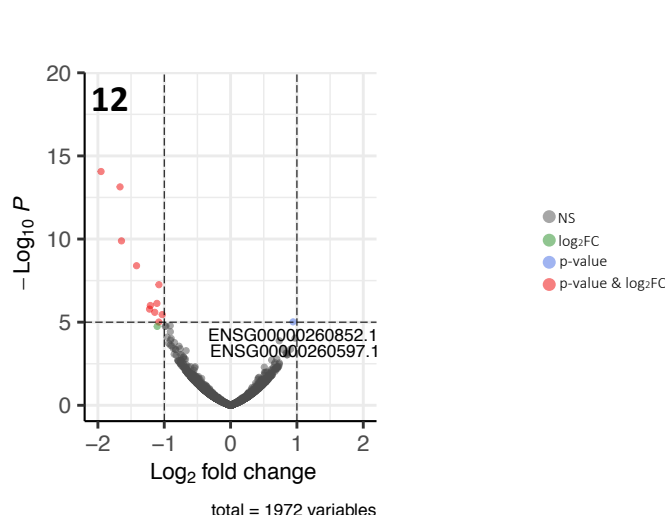


### **Sup Figure 3: Regulation of lncRNA expression and polysome association**

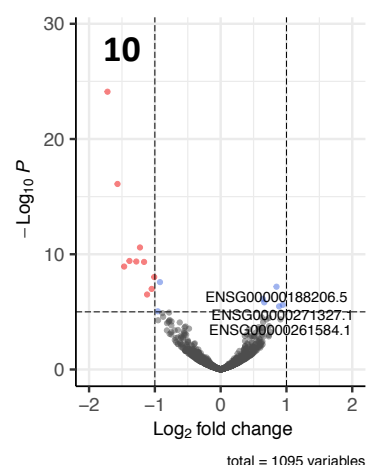
(A) Pipeline of lncRNA differential expression analysis. (B) Volcano plot displaying the significantly differentially expressed lncRNAs (labelled by their geneIDs) between Control and RA populations (Total) with  $\log_2$  fold-change cutoff=1,  $p^{\text{adj}}<0.05$ . Venn diagrams of overlap in differentially expressed lncRNAs between Total and Polysomes datasets for (C) upregulated lncRNAs and (D) downregulated lncRNAs upon differentiation. Pie charts showing breakdown by lncRNA type for lncRNAs (E) upregulated and (F) downregulated upon differentiation (Polysome) (dark purple: intergenic; magenta: anti-sense; purple: sense-overlapping; dark pink: retained intron; light pink: sense-intronic; white: uncharacterized; bright pink: NMD target).

# Sup 4

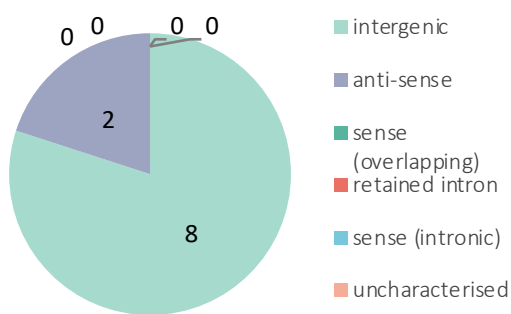
Control Total vs Control polysome-LncRNAs



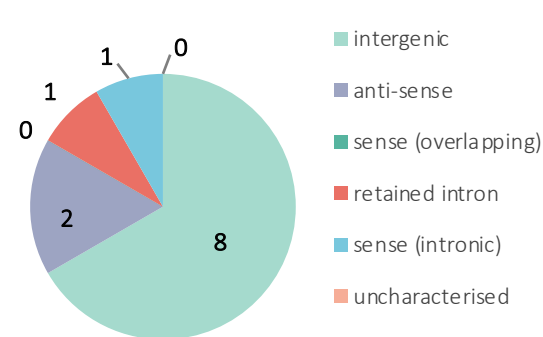
RA Total vs RA polysome-LncRNAs



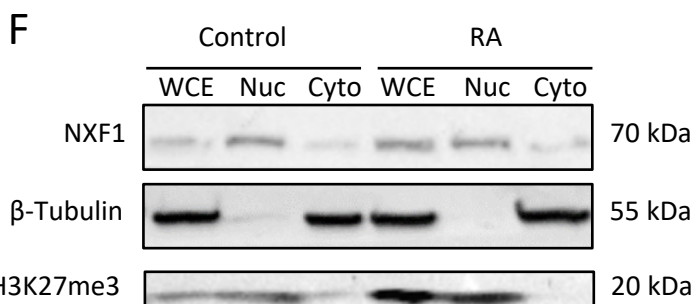
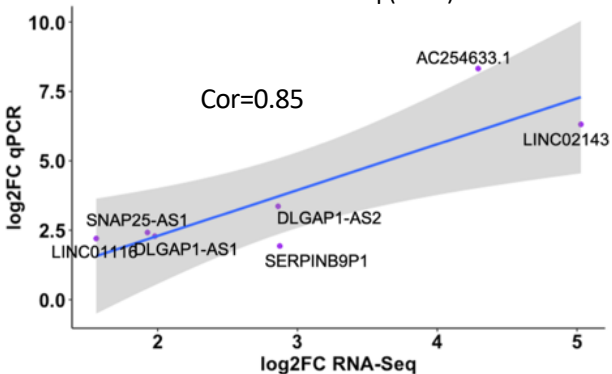
LncRNAs depleted from polysomes in RA



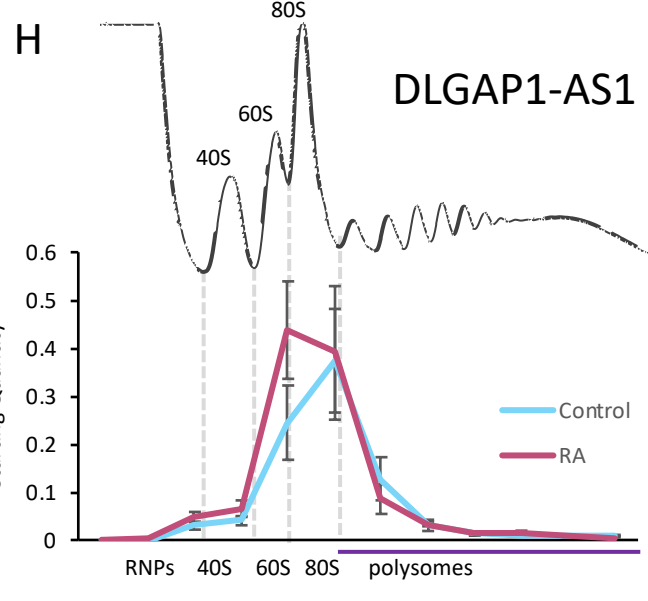
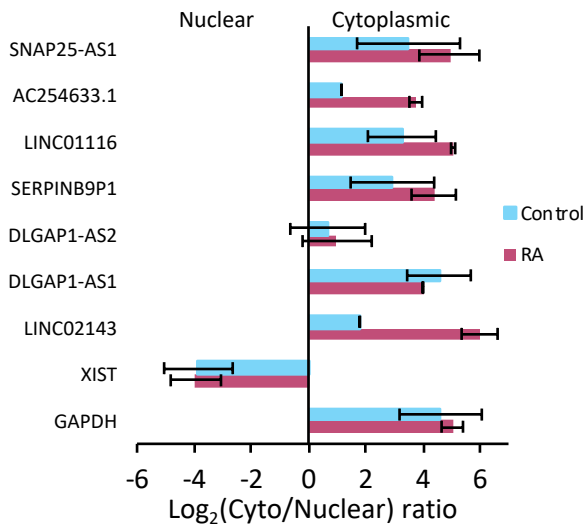
LncRNAs depleted from polysomes in Control



Correlation of log<sub>2</sub> fold-change between qPCR and RNA-Seq (total)



## G



#### Sup Figure 4: Regulation of lncRNA expression and polysome association

Volcano plots displaying the significantly differentially localised lncRNAs (labelled by their geneIDs) between Total and Polysome populations in (A) Control and (B) RA with  $\log_2$  fold-change cutoff=1,  $p^{\text{adj}}<0.05$ . Pie charts of lncRNA types present in different populations (C) depleted from polysomes in RA and (D) depleted from polysomes in Control (intergenic; anti-sense; sense-overlapping; retained intron; sense-intronic; uncharacterized; NMD target). (E) Correlation of RT-qPCR data for fold-change for lncRNAs with RNA-Seq analysis (LINC01116, LINC02143, SNAP25-AS1, DLGAP1-AS1, DLGAP1-AS2, SERPINB9P1 and AC254633.1). (F) Western blot confirming cellular fractionation with nuclear marker (H3K27me3) and cytoplasmic markers (beta-tubulin). (G) LncRNAs of interest that are induced are specifically localised to cytoplasm as shown by subcellular localisation RT-qPCR for Control and RA samples. XIST lncRNA was used as a nuclear and GAPDH mRNA as a cytoplasmic positive control ( $n=3$ , SE is plotted). (H) RT-qPCR of lncRNAs across sucrose gradient fractions indicates that DLGAP1-AS2 is found in 80S and small polysome fractions during differentiation and fractions both in control and RA treated cells ( $n=3$ , SE is plotted) On average, 63% of the transcripts is detected in the polysome fractions in Control and 49% upon differentiation.

# Figure 4

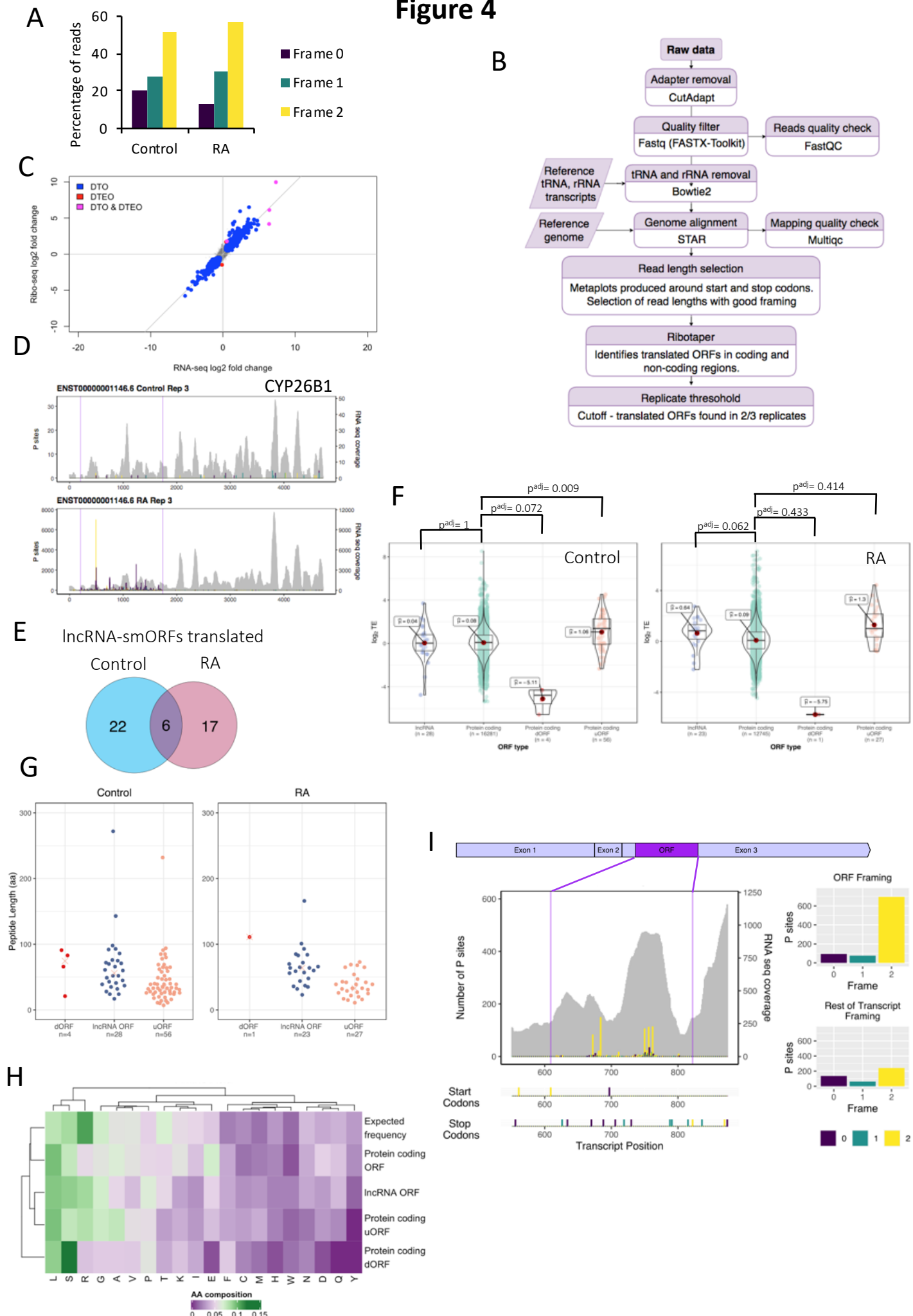


#### Figure 4: Translation of lncRNA smORFs

(A) Poly-Ribo-Seq exhibits triplet periodicity, reflecting genuine translation events. (B) Workflow for identification of translated ORFs from ribo-seq and RNA-seq, see materials and methods for details. (C) Plot of log<sub>2</sub>-fold change for each ORF in RNA (RNA-Seq) versus ribosome footprints (Ribo-Seq). DTOs (differentially transcribed ORFs) or forwarded ORFs are driven by transcriptional regulation, with significant  $\Delta$ RPF and  $\Delta$ RNA but no significant  $\Delta$ TE (blue). DTEOs (differential translation efficiency ORFs) or exclusive ORFs are driven by translational regulation, with significant  $\Delta$ RPF and  $\Delta$ TE without any significant  $\Delta$ RNA (red). DTO & DTEOs (ORFs undergoing differential transcription and translation efficiency) are either intensified; a significant  $\Delta$ TE acts with a significant  $\Delta$ RNA, or buffered; a significant  $\Delta$ TE is completely counteracting a  $\Delta$ RNA, leading to no significant  $\Delta$ RPF (pink). (D) View of Poly-Ribo-Seq data for CYP26B1. This is DTG ORF and exhibits significant  $\Delta$ RNA and  $\Delta$ RPF. (E) Venn diagram of lncRNA smORFs translated in Control and RA, with overlap. (F) Plots of Translational Efficiencies for protein-coding ORFs, lncRNA-smORFs, dORFs and uORFs. (G) Length distribution of translated ORFs in lncRNAs, dORFs and uORFs (in codons) in Control and RA. (H) Amino acid usage for smORFs compared to protein-coding ORFs and expected frequency. (I) Poly-Ribo-Seq profile for LINC01116 in RA treatment. RNA-Seq (Polysome) reads are grey and ribosome P sites in purple, turquoise and yellow according to frame. Purple lines mark beginning and end of translated smORF. All possible start and stop codons are indicated below. Framing within and outside translated smORF shown on left.

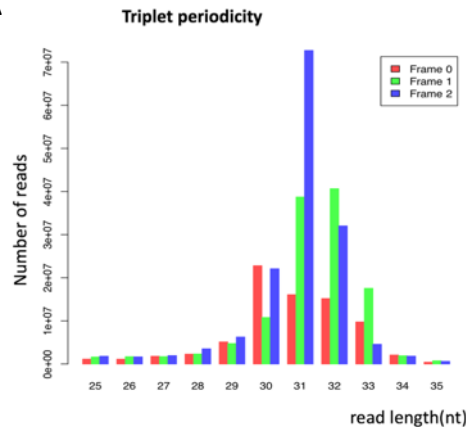
Translated ORFs	Control	RA	Overlap	Total
Protein-Coding ORFs	16,282	12,745	10,014	19,013
uORFs	56	27	12	71
dORFs	4	1	0	5
lncRNA-smORFs	28	23	6	45

**Table 1: Translation of small ORFs**

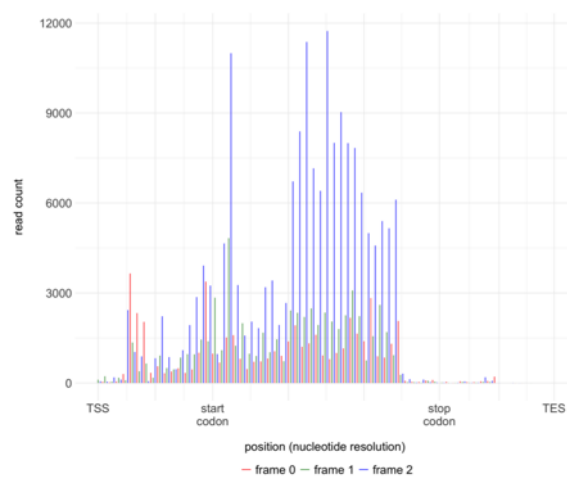
Number of ORFs detected as translated in Poly-Ribo-Seq

# Sup Fig 5

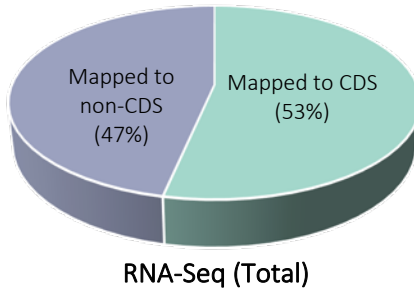
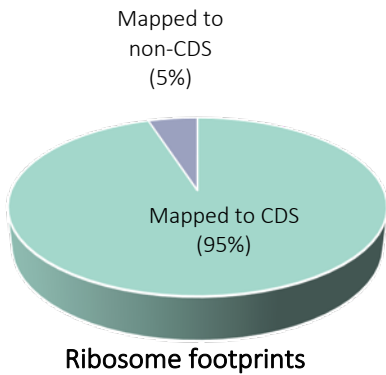
A



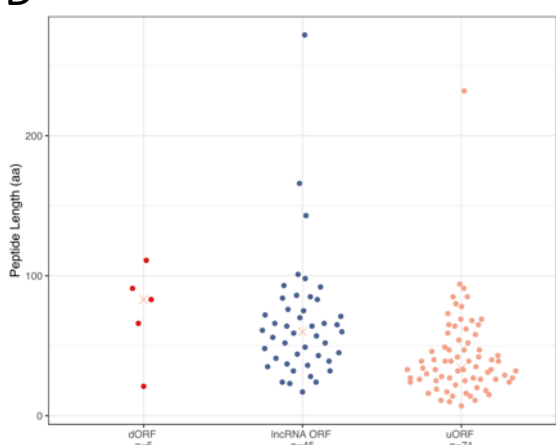
C



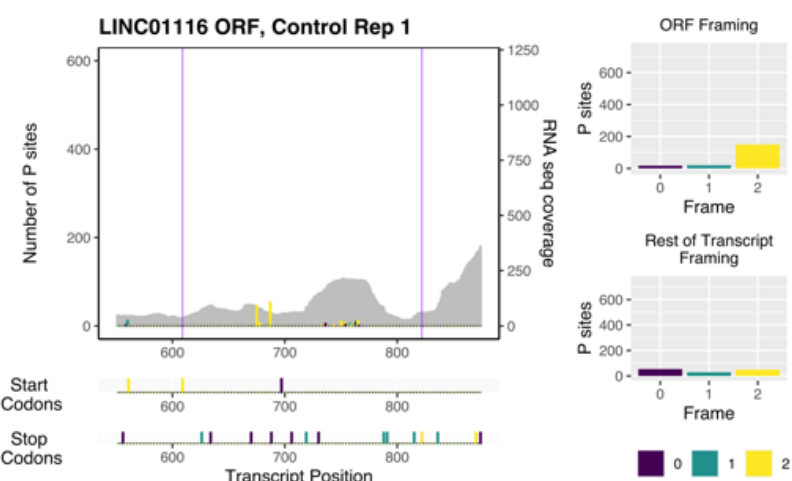
B



D



E



### Sup Figure 5: Translation of lncRNA smORFs

(A) Triplet periodicity plot for 25-35 nt reads from RA sample, replicate 3. (B) Pie charts of numbers of reads mapping to CDSs and elsewhere for ribosome footprints and RNA-Seq (Total). Values are mean of three Control replicates. (C) Metagene analysis for 33 nt reads from 33 nt reads from replicate x, Control sample. (D) Length distribution of translated ORFs in lncRNAs, dORFs and uORFs (in codons), results from Control and RA combined. (E) Example Poly-Ribo-Seq profile for LINC01116 in control treatment. RNA-Seq (Polysome) reads are grey and ribosome P sites in red, green and blue according to frame. Purple lines mark beginning and end of translated smORF. All possible start and stop codons are indicated below. Framing within and outside translated smORF shown on left.

**Sup Table 1**

Summary of triplet periodicity data for all 3 replicates, Control and RA, for 31 nt and 33 nt footprint lengths

Control	33nt long reads		
	Frame 0	Frame 1	Frame 2
rep1	22863313	49448301	21722546
rep2	2805820	2664114	2205933
rep3	15264767	27379738	7843708

RA	33nt long reads		
	Frame 0	Frame 1	Frame 2
rep1	17268000	29857839	18325348
rep2	3129165	2453330	2127290
rep3	11751674	21167199	5521907

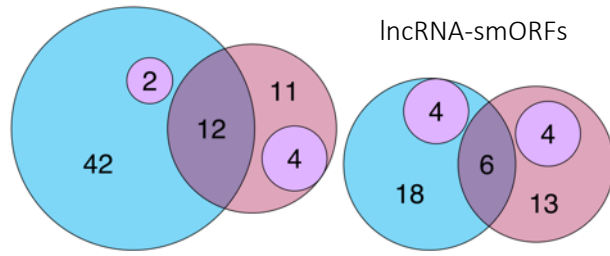
Control	31nt long reads		
	Frame 0	Frame 1	Frame 2
rep1	24005094	32426374	60624552
rep2	8362106	23604658	23159636
rep3	9924066	17280912	30882341

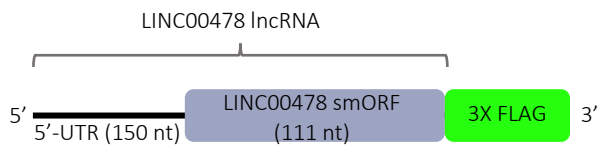
RA	31nt long reads		
	Frame 0	Frame 1	Frame 2
rep1	15605202	15497506	16166029
rep2	4896645	12171565	11646160
rep3	19042787	45325747	85476963

# Figure 5

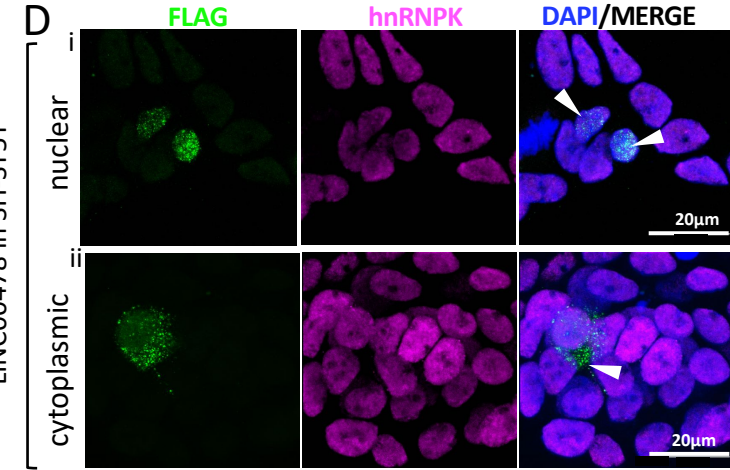
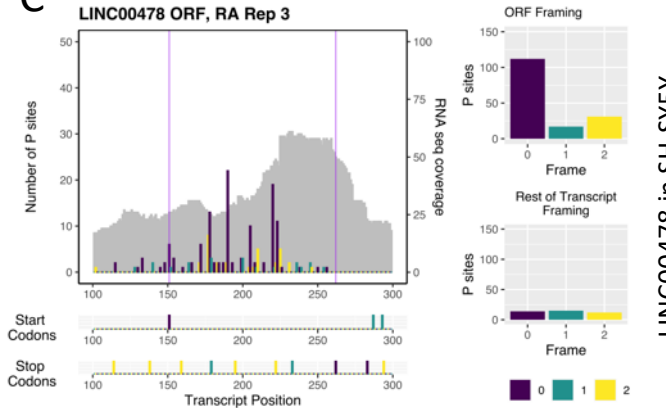
A



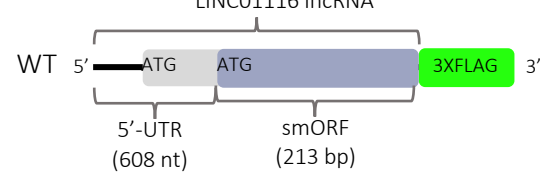
B



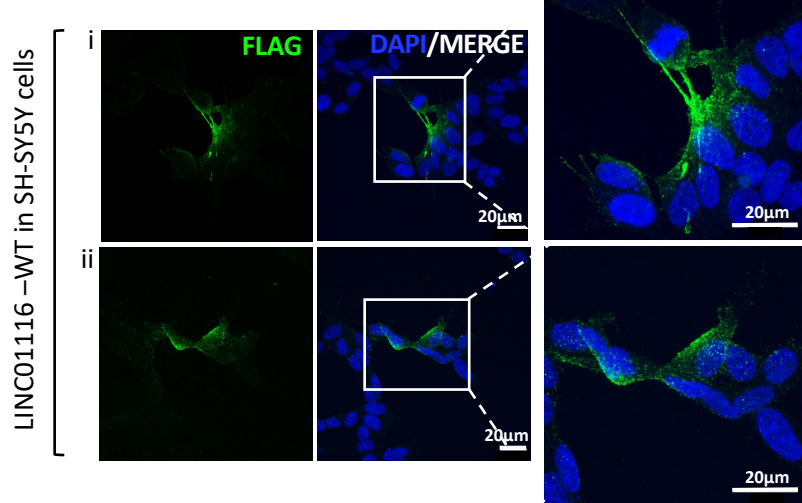
C



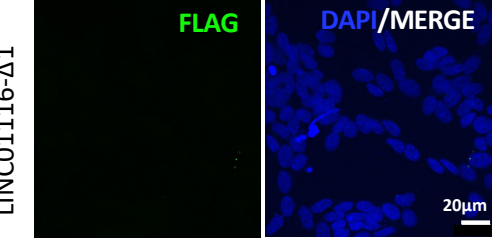
E



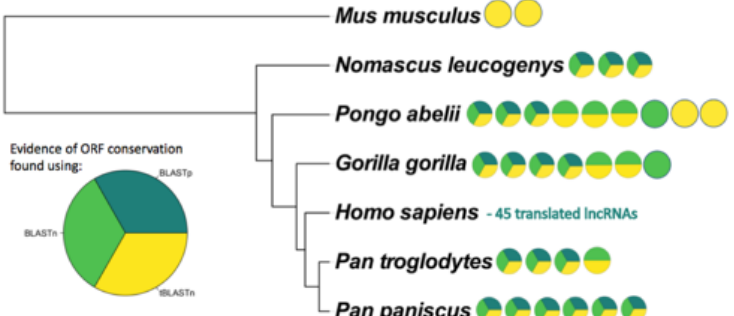
F



G



Tree scale: 10 MY



H

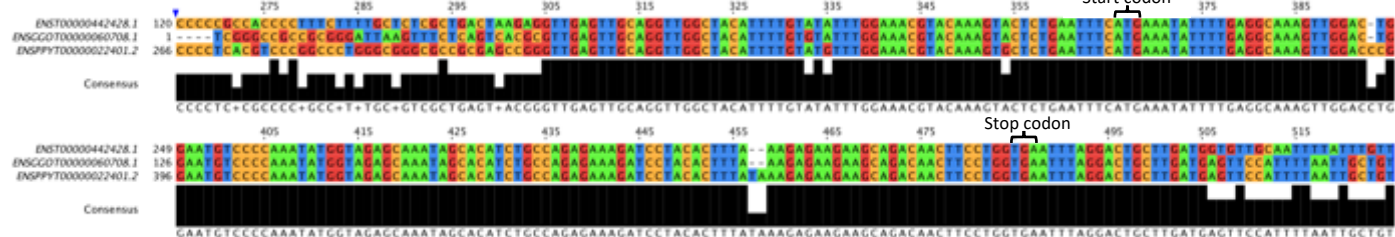
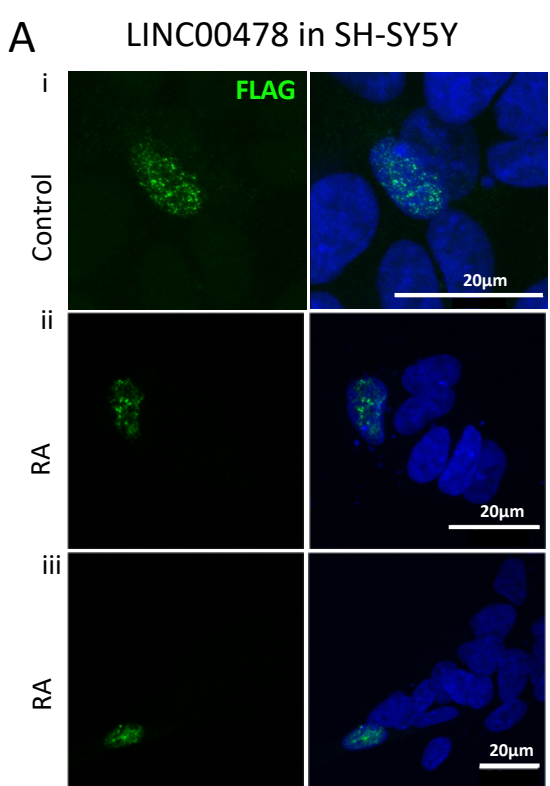
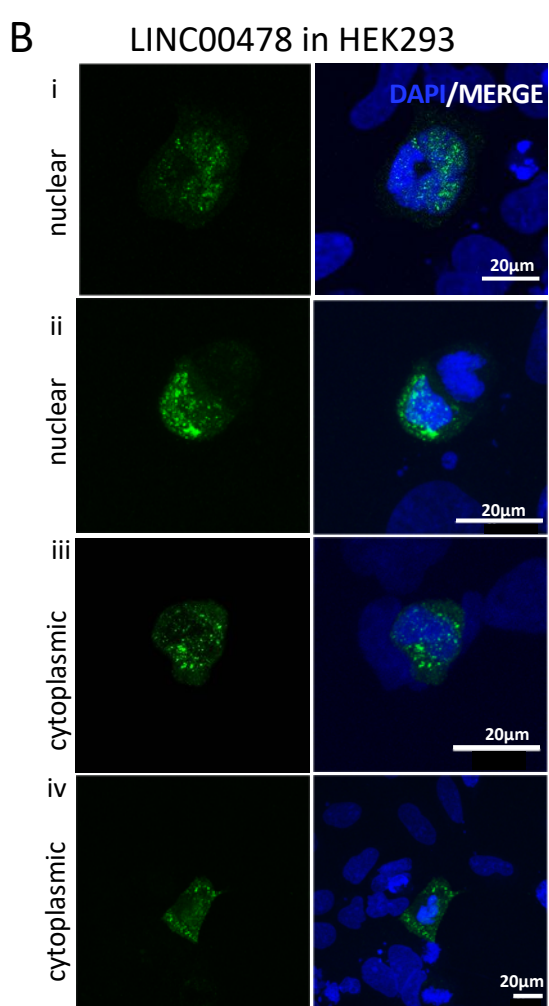


## Figure 5: Peptide production from smORFs in lncRNAs

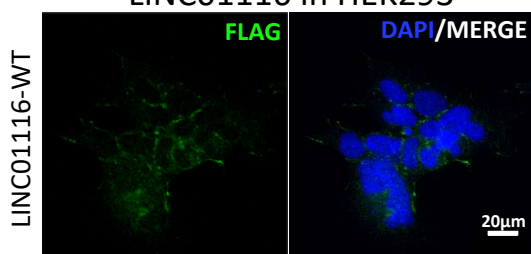
(A) Venn diagrams showing overlap in uORFs and lncRNA-smORFs detected, between our Poly-Ribo-Seq and publicly available mass spectrometry data from SH-SY5Y (purple). Control in blue, RA in pink. (B) Schematic of tagging construct for LINC00478; lncRNA sequence upstream of smORF and smORF, excluding its stop codon, cloned upstream of 3X FLAG, which is lacking its own start codon. FLAG signal is therefore dependent on smORF translation. (C) Poly-Ribo-Seq profile for LINC00478 in RA treatment. RNA-Seq (Polysome) reads are grey and ribosome P sites in purple, turquoise and yellow according to frame. Purple lines mark beginning and end of translated smORF. All possible start and stop codons are indicated below. Framing within and outside translated smORF shown on right. (D) Confocal images of FLAG-tagged LINC00478 peptide in SH-SY5Y cells (Control), showing (i) nuclear and (ii) cytoplasmic distribution, green is FLAG, magenta is hnRNP K (marking nuclei) and blue is DAPI (scale bar is 20 $\mu$ m). (E) Schematic of tagging constructs for LINC01116 (WT and start codon mutant  $\Delta$ 1). (F) Confocal images of FLAG-tagged LINC01116 peptide (WT showing cytoplasmic localisation, near cell membrane and neuritic processes (magnification of insert is 3X). (G)  $\Delta$ 1 start codon mutant, showing no FLAG signal, in SH-SY5Y cells; green is FLAG and blue is DAPI (scale bar is 20 $\mu$ m). (H) Portion of human ENST00000442428 lncRNA nt alignment with gorilla and orangutan nt sequences, showing the smORF. Alignment built in ClustalOmega (Sievers, F. et al. 2011) displayed in JalView (Waterhouse, A.M. et al. 2009). (I) Phylogram with lncRNA-smORFs for which evidence of sequence conservation were found represented as circles, coloured according to how sequence conservation was identified. Phylogram built in iTOL (Letunic, I. et al. 2006) using data from TimeTree (Kumar, S., et al. 2017), scale in 10 MYA along.



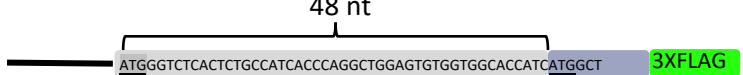
Sup 6



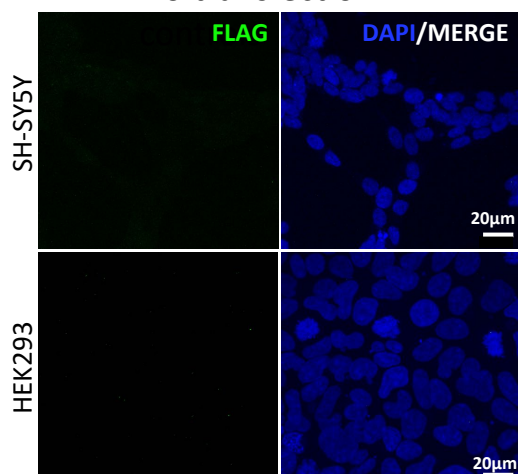
C LINC01116 in HEK293



43



## E No transfection



F

Tree scale: 10

**Mus musculus**

**Nomascus leucogenys**

**Pongo abelii**

**Gorilla gorilla**

**Homo sapiens**

**Pan troglodytes**

**Pan paniscus**

Evidence of ORF conservation found using:

BLASTp

BLASTn

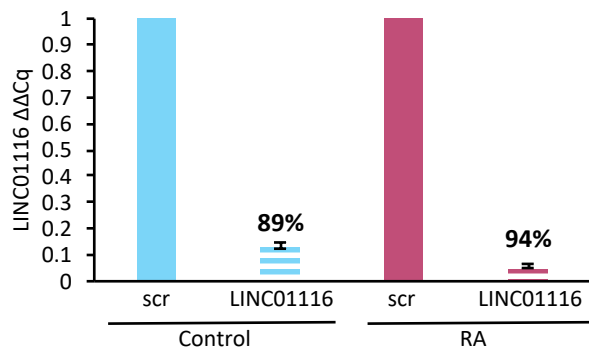
iBLASTn

## Sup Figure 6: Peptide production from smORFs in lncRNAs

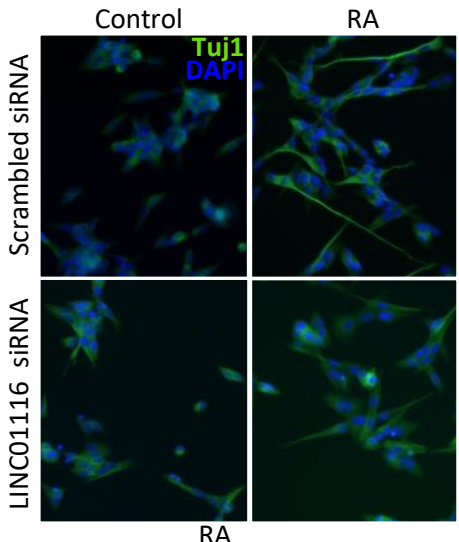
(A) Representative confocal images of FLAG-tagged LINC00478 peptide in (i) Control and (ii-iii) RA treated SH-SY5Y cells. LINC00478 exhibits nuclear distribution. (B) Representative confocal images of transfections of FLAG-tagged LINC00478 smORF in HEK293 cells; showing (i-ii) nuclear and (iii) cytoplasmic distribution, green is FLAG, and blue is DAPI (scale bar is 20 $\mu$ m). (C) Representative confocal images of FLAG-tagged LINC01116 smORF (i) WT showing cytoplasmic distribution near cell membrane and filopodia. Green is FLAG and blue is DAPI (scale bar is 16 $\mu$ m). (D) schematic of LINC01116 smORF with 2 start codons annotated. (E) Negative control (no transfection) in (i) SH-SY5Y and (ii) HEK293 cells; green is FLAG and blue is DAPI (scale bar is 20 $\mu$ m). (F) Phylogram with lncRNA-smORFs for which evidence of sequence conservation were found represented as circles, coloured according to how sequence conservation was identified. Each lncRNA-smORF with evidence of sequence conservation is shown along with which species shown conservation. Phylogram built in iTOL (Letunic, I. et al .2006) using data from TimeTree (Kumar, S. , et al. 2017), scale in 10 MYA along.

# Figure 6

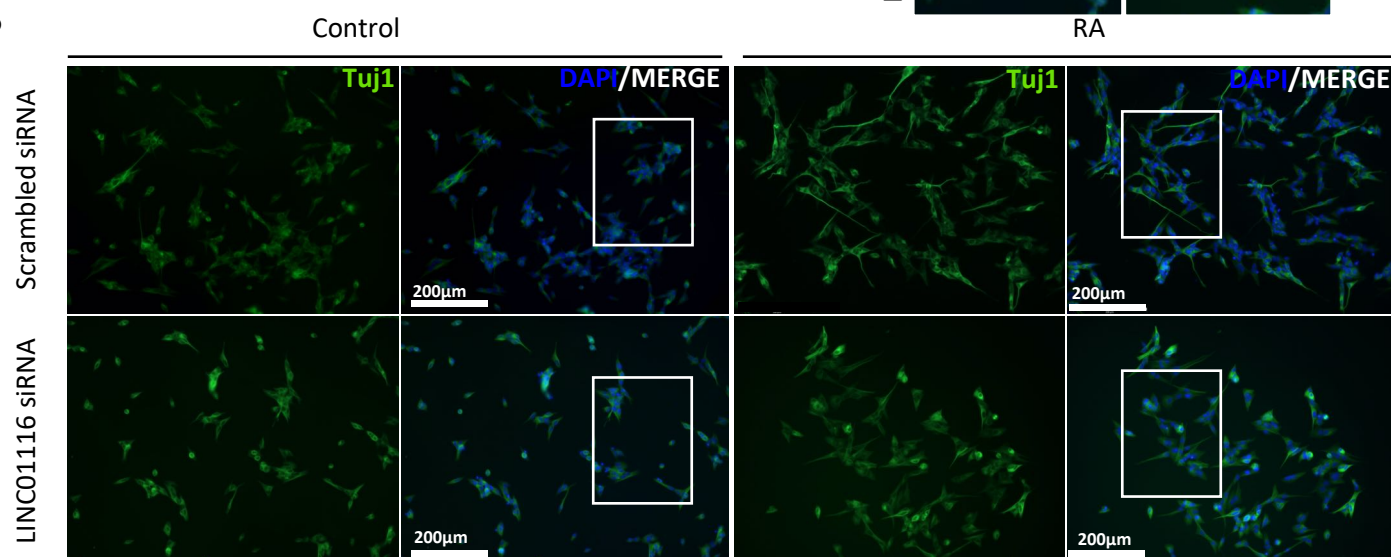
A



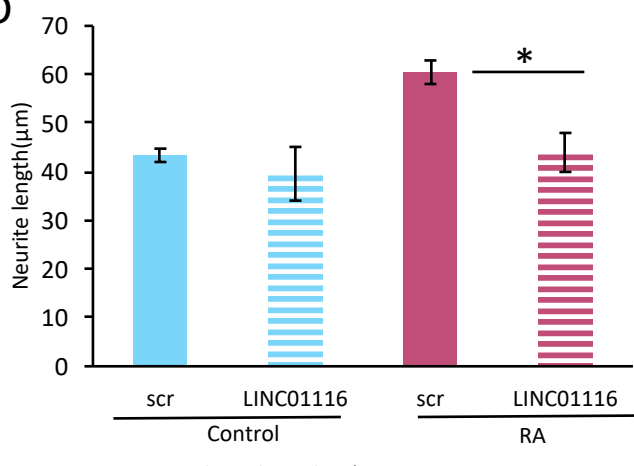
C



B

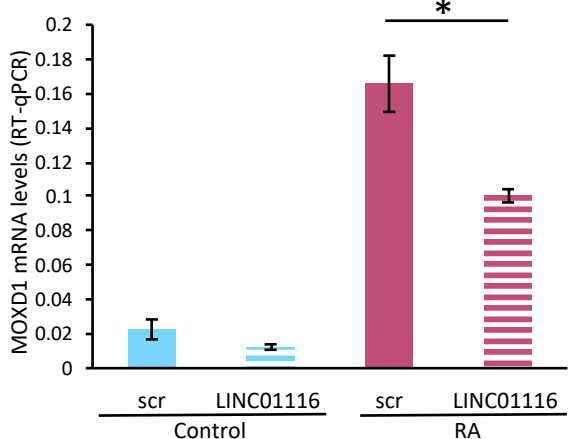


D



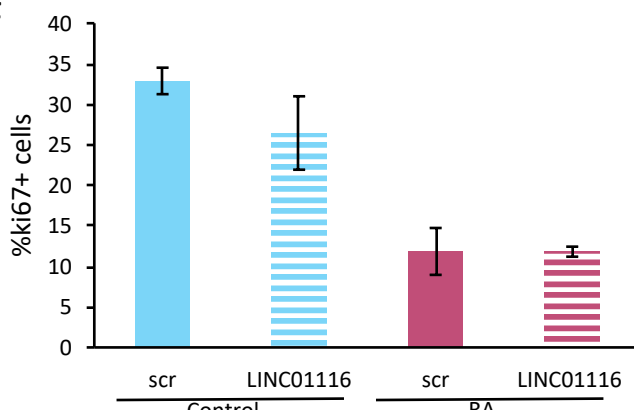
SE is plotted, Student's t-test, N=3, n>100, p<0.05

E



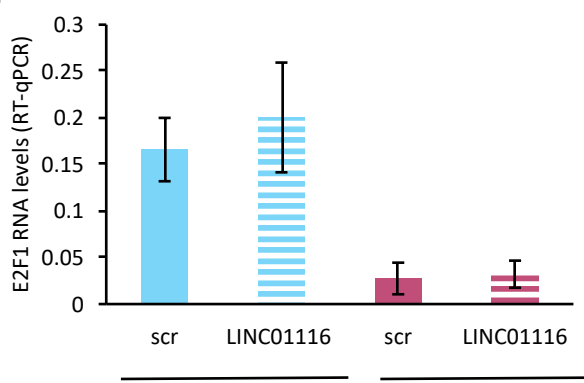
SE is plotted, Student's t-test, N=3, p<0.05

F



SE is plotted, Student's t-test, N=3, n>100, p>0.05

G



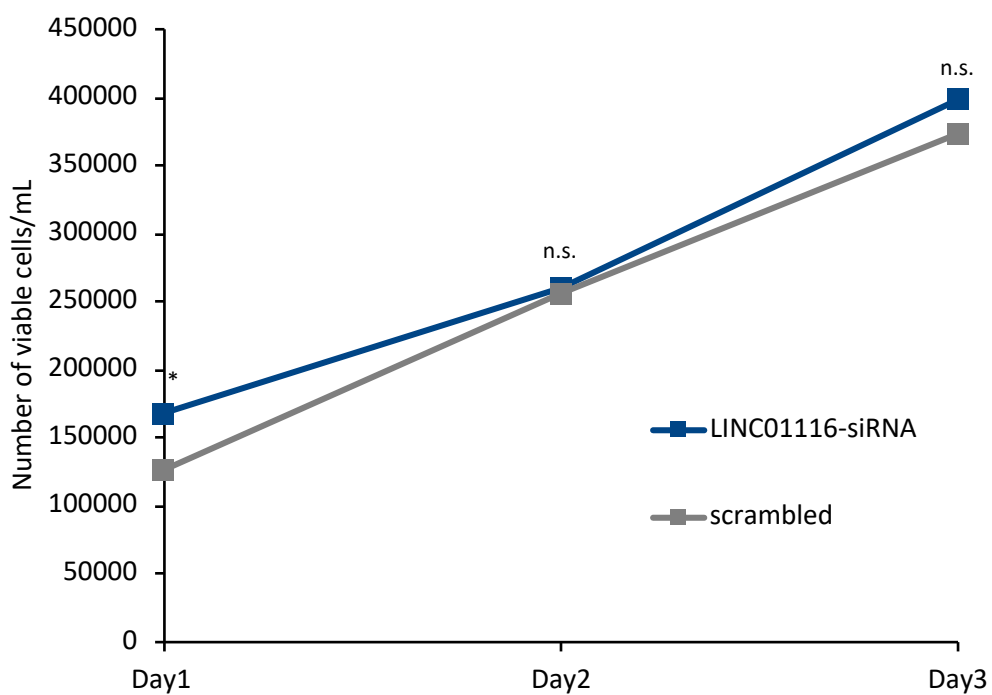
SE is plotted, Student's t-test, N=3, p>0.05

## **Figure 6: LINC01116 contributes to neuronal differentiation but does not affect cell cycle progression.**

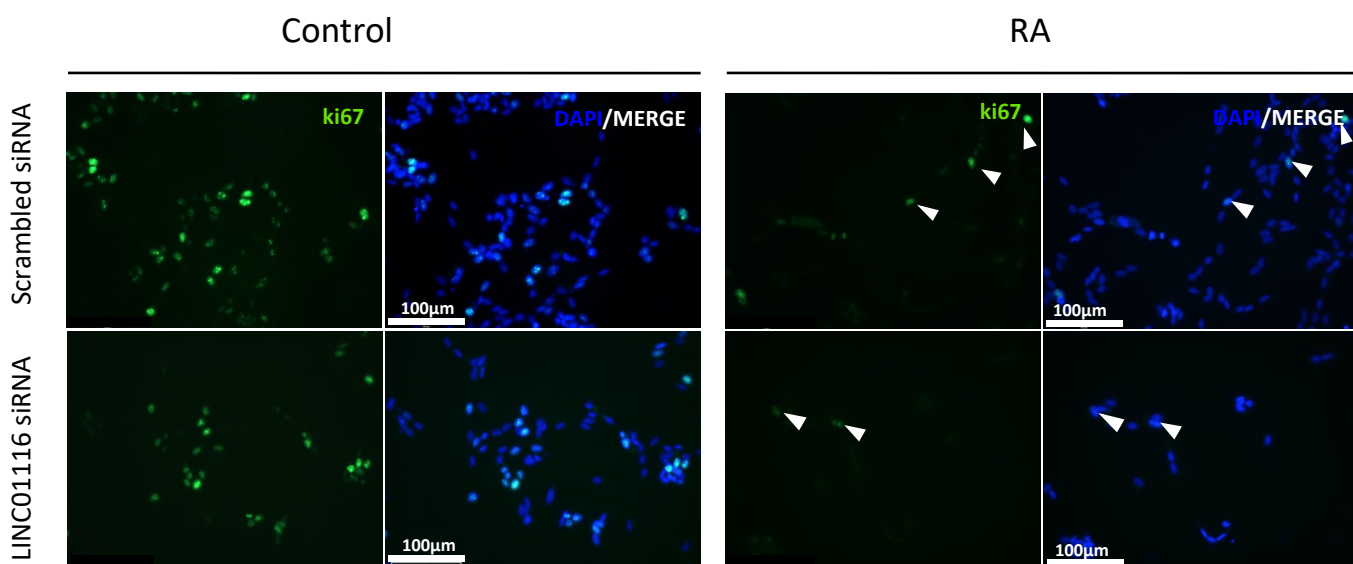
(A) LINC01116 was efficiently knocked down prior to differentiation and the knockdown is persistent throughout differentiation. (B) Representative immunofluorescence image of Control and RA SH-SY5Y cells, transfected with siRNA targeting LINC01116 and scrambled control, after staining for Tuj ( $\beta$ III-tubulin) at day 3 post-differentiation (scale bar=200 $\mu$ m). White windows magnified in (E). (C) Quantification of neurite length in Control and RA treated cells upon knockdown shows a significant reduction of neurite length in the differentiated cells that lack expression of LINC01116 (N=3 biological replicates, n>100 measurements, student's t-test p<0.05). (D) RT-qPCR of differentiation marker MOXD1 in Control and RA treated cells, transfected with siRNA targeting LINC01116 and scrambled control, shows significant reduction of MOXD1 expression in differentiated cells with reduced LINC01116 levels at day 3 post-differentiation (n=3 biological replicates, student's t-test p<0.05). (F) Quantification of proliferating cells (% of ki67+ cells) in Control and RA cells shows no effect of LINC01116 knockdown on cell proliferation (N=3 biological replicates, n>100 measurements, student's t-test p>0.05). (G) LINC01116 knockdown does not affect cell cycle progression as shown by RT-qPCR targeting cell cycle promoting transcription factor E2F1 (n=3 biological replicates, student's t-test p>0.05).

# Sup Fig 7

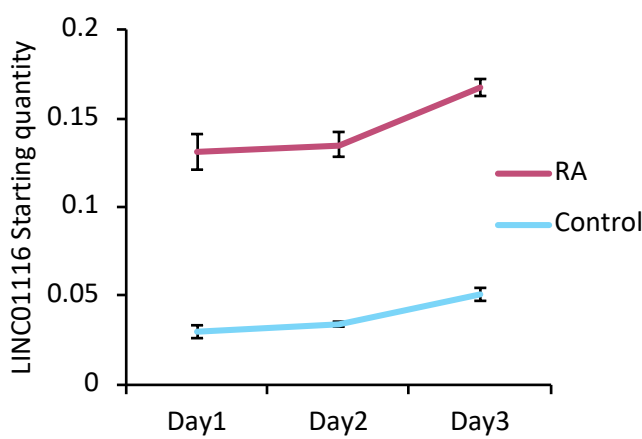
A



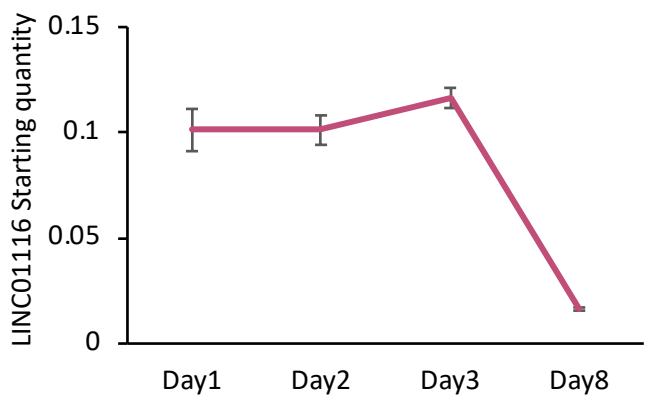
B



C



D



**Sup Figure 7: LINC01116 expression is upregulated early on upon differentiation and does not affect cell cycle progression.**

(A) LINC01116 knockdown is not cytotoxic, as shown by cell viability assay (N=3 biological replicates, n=2 technical duplicates per replicate, student's t-test  $p>0.05$ ). (B) Representative immunofluorescence of Control and RA SH-SY5Y cells, transfected with LINC01116 or scrambled siRNA, after staining for proliferation marker ki67 (arrowheads mark ki67+ cells) at day 3 post differentiation (N=3 biological replicates, n>100 measurements, student's t-test  $p>0.05$ ). Scale bar=100 $\mu$ m (C) Expression of LINC01116 lncRNA is upregulated from first day post-differentiation as shown by RT-qPCR (N=3 biological replicates, student's t-test  $p<0.05$ ). (D) LINC01116 expression levels, in phase 1 and phase 2 differentiated SH-SY5Y cells, measured by RT-qPCR. LINC01116 levels decrease ~6-fold during phase 2 differentiation (n=3, standard deviation is plotted).